Electronic Research Archive

https://www.aimspress.com/journal/era

ERA, 34(10): 7362–7391.
DOI: 10.3934/era.2026318
Received: 17 June 2026
Revised: 04 August 2026
Accepted: 14 August 2026
Published: 27 August 2026

Research article

Dynamical analysis of a Filippov pest-natural enemy model incorporating fear and prey refuge

Wen Sun and Zhongyi Xiang*

School of Mathematics and Statistics, Hubei Minzu University, Enshi 445000, China

* **Correspondence:** Email: yfxiang2007@163.com.

Abstract: This paper establishes a Filippov integrated pest management model with the fear effect and prey refuge, aiming to investigate economic-threshold-based intermittent control strategies and their dynamical behavior. First, the existence and local stability of the equilibria of the two subsystems are discussed, and the nonsmooth dynamics of the Filippov system are analyzed. Furthermore, sliding bifurcations, boundary equilibrium bifurcations, and global sliding bifurcations are investigated through numerical simulations. The results indicate that the control effect is highly sensitive to the threshold value, and as the threshold varies, the system exhibits a series of complex bifurcation phenomena. Furthermore, pest refuge behavior may weaken the effectiveness of control measures. Although the fear effect can suppress pest growth, an excessively strong fear effect may reduce prey availability for natural enemies, thereby limiting their population growth.

Keywords: threshold strategy; Filippov system; sliding mode; fear effect; prey refuge

1. Introduction

Pests pose multiple threats to agricultural production and the natural environment by feeding on crops and transmitting diseases. From both an ecological perspective and in light of current technological capabilities, the complete eradication of pests is not realistic. In agricultural practice, a more reasonable approach is to adopt scientific and effective integrated management strategies to keep pest populations below the economic injury level. Integrated pest management (IPM) is a pest control strategy that combines multiple methods and techniques, aiming to achieve effective pest suppression and sound management while reducing negative environmental and ecological impacts. IPM is designed to manage pests through the coordinated application of multiple control approaches. These approaches are determined by the biological features of the target pests, local environmental factors, and crop growth status, so that pest management can meet economic, ecological, and social objectives simultaneously [1–4]. In recent years, the dynamical behavior of Filippov systems has attracted

increasing attention in biological applications. Cortés-García [5–7] investigated threshold-dependent dynamics in Filippov predator-prey systems. These studies considered Gause models with predator competition or hunting cooperation under different prey-density regimes, as well as a Leslie-Gower model with predator harvesting at high densities. Currently, Filippov systems have been widely applied to epidemiological models [8–12], ecological and predator-prey systems [13–15], and biological control problems [16–20]. These studies provide a useful mathematical framework for describing systems with switching control strategies.

Building upon these developments, Filippov pest management models have attracted considerable attention. Zhou et al. [21] investigated a nonsmooth Filippov pest management model with a constant release rate, and systematically analyzed its global dynamics and bifurcation behavior, providing a theoretical basis for integrated pest management under threshold-based control. Qin, Kang, and their collaborators [22, 23] developed Filippov pest management models incorporating a constant release rate and a group defense mechanism to characterize the effects of integrated pest management on the dynamical behavior of the system. Arafa et al. [24] further introduced time delay and studied delay-induced stability changes and nonsmooth bifurcations.

However, most existing pest management models do not simultaneously take into account the fear effect of pests toward natural enemies and the refuge-use behavior of pest populations. A large body of experimental and theoretical studies has shown that predators affect prey populations not only through direct predation, but also by inducing fear effects that alter prey foraging, reproduction, and growth behaviors. For example, experiments conducted by Zanette et al. [25] during the breeding season of North American song sparrows found that, in areas with higher predation risk, song sparrows were more likely to build nests in concealed locations and reduce their foraging activity, which led to an approximately 40% reduction in offspring production. This result indicates that the perception of predation risk can significantly influence prey population dynamics and, in turn, affect ecosystem stability [26–30]. On the other hand, in nature, many pest populations actively seek out and utilize refuges because of the fear of predation by natural enemies, such as hiding beneath plant leaves, in the soil, or under tree bark. These refuges provide physical protection, enabling pests to escape predation threats and avoid unfavorable environmental conditions [31–34]. For example, western flower thrips exhibit pronounced refuge-seeking behavior in response to the perceived presence of natural enemies. When natural enemies such as predatory flower bugs are present, western flower thrips reduce their activity on exposed plant surfaces and instead move to concealed sites, such as the undersides of leaves and deeper layers of the plant canopy. They may also use web structures produced by spider mites on leaves as safe refuges, thereby reducing the risk of predation [35, 36].

In recent years, many studies have examined how biological factors and ecological processes influence population dynamics. Mokni and Ch-Chaoui [37, 38] investigated the effects of strong Allee effects and evolutionary adaptation on the stability and bifurcations of Ricker-type population models. Ahmidi et al. [39] and Benali et al. [40] examined the influences of prey harvesting and immigration on predator-prey dynamics, respectively. By combining analytical analysis with numerical simulations, Zhang et al. [41] explored the effects of two antipredator factors, predation-induced fear effects and prey refuge behavior, on the dynamical characteristics of predator-prey systems. Hamdallah and Arafa [42] further developed a Filippov predator-prey model with a switching prey-refuge mechanism. Its switching condition depends on the prey-to-predator density ratio. Prey

enter the refuge under relatively high predation risk when this ratio falls below a prescribed threshold and leave the refuge to forage when the ratio exceeds the threshold.

Although existing studies have incorporated the fear effect and prey refuge behavior into predator–prey systems, their combined influence in economic-threshold-based pest management remains insufficiently investigated. Moreover, the switching condition in Hamdallah and Arafa's model [42] depends on the prey-to-predator density ratio and mainly describes refuge switching, whereas practical pest-management measures are generally activated when pest density reaches an economic threshold. These gaps motivate us to develop a Filippov pest-natural enemy model that simultaneously incorporates the fear effect and prey refuge behavior and adopts pest population density as its switching condition. The main contributions of this study are as follows: The fear effect and pest refuge behavior are simultaneously incorporated into a Filippov system to characterize economic-threshold-based integrated pest management; the system's sliding dynamics and nonsmooth bifurcation behavior are systematically analyzed; and the combined effects of the economic threshold, fear effect, and refuge behavior on pest-control outcomes are further elucidated. These results provide a new theoretical basis for developing threshold-based integrated pest management strategies.

The structure of this paper is as follows. Section 2 presents the formulation of the economic-threshold-based Filippov pest-management model and explains the biological significance of model parameters. In Section 3, we prove the positivity and boundedness of solutions and discuss the existence and stability of the equilibria of subsystems S_1 and S_2. Section 4 investigates sliding-mode dynamics, derives existence conditions for various equilibria of the Filippov system, and analyzes the stability of pseudo-equilibria. Section 5 studies sliding bifurcations, boundary equilibrium bifurcations, and global sliding bifurcations via numerical simulations. Section 6 analyzes the fear effect on system (3.2) and provides parameter sensitivity analysis. Finally, Section 7 summarizes the main results and discusses their biological implications.

2. Model formulation

The present study is based on the continuous predator-prey model incorporating fear and refuge effects proposed by Zhang et al. [41]. Unlike the switching condition proposed in Hamdallah and Arafa's model [42], the switching condition adopted here is determined by pest population density, and pest control measures are activated only when pest density reaches the threshold level.

When the pest density remains below the economic threshold ET, no control measure is implemented. Once the pest density exceeds ET, pesticide application and the constant release of natural enemies are activated. Accordingly, the following control model is obtained:

$$\begin{cases} \left.\begin{aligned} \frac{dx}{dt} &= \frac{rx}{1+\varphi y} - \frac{rx^2}{K} - \frac{\beta(1-n)xy}{1+b(1-n)x}, \\ \frac{dy}{dt} &= \frac{c\beta(1-n)xy}{1+b(1-n)x} - \delta y, \end{aligned}\right\} x < ET, \\ \left.\begin{aligned} \frac{dx}{dt} &= \frac{rx}{1+\varphi y} - \frac{rx^2}{K} - \frac{\beta(1-n)xy}{1+b(1-n)x} - a_1 x, \\ \frac{dy}{dt} &= \frac{c\beta(1-n)xy}{1+b(1-n)x} - \delta y + a_2, \end{aligned}\right\} x > ET, \end{cases} \tag{2.1}$$

where x and y denote the densities of the pest and natural enemy populations, respectively; r is the intrinsic growth rate of the pest; K is the environmental carrying capacity of the pest; β is the predation coefficient in the Holling type-II functional response, and b is the saturation coefficient associated with handling time; δ is the natural enemy mortality rate; c is the conversion efficiency of consumed pests into the growth of the natural enemy; ET denotes the economic threshold; and a_1 denotes the pesticide-induced per capita mortality rate of the pest population, whereas a_2 denotes the constant release rate of natural enemies. Throughout this paper, we assume that $r > a_1$, ensuring that pesticide application alone is insufficient to eradicate the pest population.

From an ecological perspective, the fear function $\frac{1}{1+\varphi y}$ describes the suppression of pest growth caused by the perceived presence of natural enemies. Since $y > 0$ and $\varphi > 0$, it satisfies $0 < \frac{1}{1+\varphi y} < 1$. Its value decreases as the density of natural enemies increases, indicating stronger suppression of pest growth. The parameter $\varphi > 0$ measures the intensity of the fear effect. The term $\frac{rx}{1+\varphi y}$ represents the reduction in pest reproduction caused by fear of natural enemies, whereas $-\frac{rx^2}{K}$ describes density-dependent intraspecific competition. In this study, we assume that the fear effect suppresses the reproductive or growth activities of pests but does not directly alter intraspecific competition caused by limitations in resources and space.

The refuge parameter $n \in [0, 1)$ represents the proportion of pests protected by refuges, so only the remaining proportion $1 - n$ is exposed to predation.

The proposed model is formulated as a dimensional system, and all terms in the two equations are dimensionally consistent, with each term representing the change in population density per unit time.

The model can be written as:

$$\begin{cases} \dfrac{dx}{dt} = \dfrac{rx}{1+\varphi y} - \dfrac{rx^2}{K} - \dfrac{\beta(1-n)xy}{1+b(1-n)x} - \varepsilon a_1 x, \\ \dfrac{dy}{dt} = \dfrac{c\beta(1-n)xy}{1+b(1-n)x} - \delta y + \varepsilon a_2, \end{cases} \tag{2.2}$$

where

$$\varepsilon = \begin{cases} 0, & H(Z) = x - ET < 0, \\ 1, & H(Z) = x - ET > 0. \end{cases} \tag{2.3}$$

Set $Z(t) = (x(t), y(t))^T$ and introduce the switching function $H(Z) = x - ET$. The switching condition $H(Z) = 0$ separates the nonnegative phase plane into two domains, $G_1 = \{Z \in \mathbb{R}^2_+ : H(Z) < 0\}$, $G_2 = \{Z \in \mathbb{R}^2_+ : H(Z) > 0\}$. The corresponding switching boundary is given by $\Sigma = \{Z \in \mathbb{R}^2_+ : H(Z) = 0\}$.

Accordingly, systems (2.2) and (2.3) can be reformulated as the following Filippov system:

$$\frac{dZ(t)}{dt} = \begin{cases} F_{G_1}(Z), & Z \in G_1, \\ F_{G_2}(Z), & Z \in G_2, \end{cases} \tag{2.4}$$

where

$$F_{G_1}(Z) = \begin{bmatrix} \dfrac{rx}{1+\varphi y} - \dfrac{rx^2}{K} - \dfrac{\beta(1-n)xy}{1+b(1-n)x} \\ \dfrac{c\beta(1-n)xy}{1+b(1-n)x} - \delta y \end{bmatrix},$$

and

$$F_{G_2}(Z) = \begin{bmatrix} \dfrac{rx}{1+\varphi y} - \dfrac{rx^2}{K} - \dfrac{\beta(1-n)xy}{1+b(1-n)x} - a_1 x \\ \dfrac{c\beta(1-n)xy}{1+b(1-n)x} - \delta y + a_2 \end{bmatrix}.$$

For convenience, we denote the two subsystems associated with G_1 and G_2 by S_1 and S_2, respectively.

3. Preliminaries

3.1. Positivity and boundedness of solutions

Lemma 1. *If $x(0) > 0$ and $y(0) > 0$, then all possible solutions of system* (2.4) *are positive.*

Proof. Let $F(x, y) = \frac{r}{1+\varphi y} - \frac{rx}{K} - \frac{\beta(1-n)y}{1+b(1-n)x} - \varepsilon a_1$. Then the first equation of system (2.2) can be written as $\frac{dx}{dt} = xF(x, y)$. Hence, we obtain $x(t) = x(0)\exp\left(\int_0^t F(x(s), y(s))\, ds\right) > 0$, since $x(0) > 0$. Therefore, $x(t) > 0$ for all $t \geq 0$.

Next, we prove that $y(t) > 0$. Suppose, for contradiction, that there exists $t_3 > 0$ such that $y(t_3) \leq 0$. By continuity, there exists a first time $t_4 \in (0, t_3]$ such that $y(t_4) = 0$, and $y(t) > 0$ for all $t \in [0, t_4)$. From system (2.2), we have

$$\frac{dy}{dt} = \frac{c\beta(1-n)xy}{1+b(1-n)x} - \delta y + \varepsilon a_2 \geq -\delta y, \qquad t \in [0, t_4].$$

By a differential inequality, it follows that $y(t_4) \geq y(0)\exp(-\delta t_4)$, which contradicts $y(t_4) = 0$. Therefore, $y(t) > 0$ for all $t \geq 0$. □

Lemma 2. *Assume that the solution of system* (2.4) *with initial value $(x(0), y(0)) = (x_0, y_0)$, $x_0 > 0, y_0 > 0$, exists for all $t \geq 0$. Then this solution is bounded on $[0, \infty)$.*

Proof. From system (2.2), we have $\frac{dx}{dt} \leq rx - \frac{rx^2}{K}$. Hence, when $x > K$, it follows that $\frac{dx}{dt} < 0$. Therefore, for all $t \geq 0$, $0 < x(t) \leq \max\{x_0, K\}$, which shows that $x(t)$ is bounded. Next, we construct a Lyapunov function $W(t) = x(t) + \frac{1}{c}y(t)$. Differentiating $W(t)$ along the solutions of the system, we obtain

$$\begin{aligned} \frac{dW}{dt} &= \frac{dx}{dt} + \frac{1}{c}\frac{dy}{dt} \\ &= \frac{rx}{1+\varphi y} - \frac{rx^2}{K} - \varepsilon a_1 x - \frac{\delta}{c}y + \frac{\varepsilon a_2}{c} \\ &\leq rx - \frac{rx^2}{K} - \frac{\delta}{c}y + \frac{a_2}{c} \\ &\leq rK\left(1 - \frac{x}{K}\right) - \frac{\delta}{c}y + \frac{a_2}{c} \\ &= \left(rK + \frac{a_2}{c}\right) - rx - \frac{\delta}{c}y. \end{aligned}$$

Let $\eta = \min\{r, \delta\} > 0$, then

$$\frac{\mathrm{d}W}{\mathrm{d}t} \leq \left(rK + \frac{a_2}{c}\right) - \eta W.$$

Let $A = \left(rK + \frac{a_2}{c}\right)$, then $\frac{dW}{dt} \le A - \eta W$, and by the comparison principle, it follows that

$$W(t) \le W(0)e^{-\eta t} + \frac{A}{\eta}(1 - e^{-\eta t}), \qquad t \ge 0.$$

Hence, $W(t) \le \max\left\{W(0), \frac{A}{\eta}\right\}$. Since $x(t) \le W(t)$ and $y(t) \le cW(t)$, the solution $(x(t), y(t))$ is also bounded on $[0, \infty)$. □

3.2. Dynamics of the subsystem S_1

The subsystem S_1 is given by

$$\begin{cases} \dfrac{dx}{dt} = \dfrac{rx}{1+\varphi y} - \dfrac{rx^2}{K} - \dfrac{\beta(1-n)xy}{1+b(1-n)x}, \\ \dfrac{dy}{dt} = \dfrac{c\beta(1-n)xy}{1+b(1-n)x} - \delta y. \end{cases} \tag{3.1}$$

For simplicity, we impose the following assumptions: It is assumed that

(H1) $c\beta - b\delta > 0$,

(H2) $1 - \dfrac{\delta}{K(c\beta - b\delta)} < n < 1$,

(H3) $1 - \dfrac{b\delta + c\beta}{bK(c\beta - b\delta)} \le n < 1 - \dfrac{\delta}{K(c\beta - b\delta)}$,

(H4) $0 \le n < 1 - \dfrac{b\delta + c\beta}{bK(c\beta - b\delta)}$,

(H5) $\varphi > \varphi^* := \dfrac{Kb(c\beta - b\delta)^2(1-n)^2(Kb(1-n)(c\beta - b\delta) - (b\delta + c\beta))}{\beta c^2 r(b\delta + c\beta)}$.

Since the dynamics of subsystem S_1 have already been analyzed in [41], only the results needed for the subsequent discussion are summarized here. Under these assumptions, subsystem S_1 may admit three equilibria: the trivial equilibrium $E_0 = (0, 0)$, the boundary equilibrium $E^0_{S_1} = (K, 0)$, and the positive equilibrium $E^*_{S_1} = (x^*, y^*)$. The coordinates of the positive equilibrium satisfy

$$x^* = \frac{\delta}{(1-n)(c\beta - b\delta)},$$

$$y^* = \frac{1}{2\varphi}\left(\sqrt{\Delta} - 1 - \frac{c\varphi\delta r}{K(c\beta - b\delta)^2(1-n)^2}\right),$$

with

$$\Delta = \left(1 - \frac{c\delta\varphi r}{K(1-n)^2(c\beta - b\delta)^2}\right)^2 + \frac{4c\varphi r}{(1-n)(c\beta - b\delta)}.$$

Lemma 3. *The trivial equilibrium point $E_0 = (0, 0)$ is a saddle point. If $(H1)$ does not hold, or if $(H1)$ and $(H2)$ hold simultaneously, then the boundary equilibrium point $E^0_{S_1}$ is locally asymptotically stable.*

Lemma 4. *The positive equilibrium point $E^*_{S_1}$ exists when the boundary equilibrium point $E^0_{S_1}$ is unstable, whereas $E^*_{S_1}$ does not exist when $E^0_{S_1}$ is locally asymptotically stable. Furthermore, if* $(H3)$ *holds, or if* $(H4)$ *and* $(H5)$ *hold simultaneously, then the positive equilibrium point $E^*_{S_1}$ is locally asymptotically stable.*

The assumptions (H1)–(H5) correspond to different parameter regimes and are not required to hold simultaneously. In particular, under assumption (H1), conditions (H2), (H3), and (H4) describe different ranges of the refuge parameter n, each of which is associated with a distinct dynamical scenario. When (H1) and (H2) hold simultaneously, the equilibrium $E^0_{S_1}$ is locally asymptotically stable. When (H1) and (H3) hold simultaneously, the positive equilibrium $E^*_{S_1}$ is locally asymptotically stable. Moreover, the simultaneous validity of (H1), (H4), and (H5) also guarantees the local asymptotic stability of $E^*_{S_1}$.

For example, let $r = 1.4$, $K = 10, \beta = 0.5$, $b = 0.5$, $c = 0.4$, and $\delta = 0.25$. Then $c\beta - b\delta = 0.075 > 0$, so (H1) holds. Moreover, $n = 0.80$ satisfies (H2), $n = 0.25$ satisfies (H3), and $(n, \varphi) = (0.10, 0.05)$ satisfies (H4)–(H5). These parameter values are biologically reasonable.

From a biological perspective, the instability of $E_0 = (0, 0)$ indicates that the simultaneous extinction of both populations cannot be maintained. The stability of $E^0_{S_1} = (K, 0)$ means that the natural enemy population eventually becomes extinct, while the pest population approaches its environmental carrying capacity K. Thus, natural predation alone is insufficient to control the pest. In contrast, the stability of $E^*_{S_1}$ indicates the long-term coexistence of pests and natural enemies under natural regulation.

3.3. Dynamics of the subsystem S_2

When $x > ET$, subsystem S_2 can be written as

$$\begin{cases} \dfrac{dx}{dt} = \dfrac{rx}{1+\varphi y} - \dfrac{rx^2}{K} - \dfrac{\beta(1-n)xy}{1+b(1-n)x} - a_1 x, \\ \dfrac{dy}{dt} = \dfrac{c\beta(1-n)xy}{1+b(1-n)x} - \delta y + a_2. \end{cases} \tag{3.2}$$

This subsystem has a boundary equilibrium, namely the pest-eradication equilibrium $E^0_{S_2}\left(0, \frac{a_2}{\delta}\right)$.

Next, we proceed to solve for the interior equilibrium points of subsystem S_2. From the first equation of (3.2), we have

$$K\varphi\beta(1-n)y^2 + \Big[\varphi(1+b(1-n)x)(rx+Ka_1) + K\beta(1-n)\Big]y + (1+b(1-n)x)(rx-rK+Ka_1) = 0. \tag{3.3}$$

When $x < K\left(1 - \frac{a_1}{r}\right)$, the pest nullcline is given by

$$y = M_1(x) = \frac{\sqrt{\Delta} - [K\beta(1-n) + \varphi(1+b(1-n)x)(rx+Ka_1)]}{2K\varphi\beta(1-n)}, \tag{3.4}$$

with

$$\Delta = [K\beta(1-n) - \varphi(1+b(1-n)x)(rx+Ka_1)]^2 + 4rK^2\varphi\beta(1-n)(1+b(1-n)x).$$

Let the second equation of (3.2) be set to zero, which gives the natural-enemy nullcline

$$y = M_2(x) = \frac{a_2}{\delta - \dfrac{c\beta(1-n)x}{1+b(1-n)x}} = \frac{a_2(1+b(1-n)x)}{\delta(1+b(1-n)x) - c\beta(1-n)x}. \tag{3.5}$$

Since obtaining the intersections analytically is comparatively difficult, a graphical approach is employed to analyze the number of equilibrium points. The intersections of Eqs (3.4) and (3.5) correspond to the interior equilibria of the model. Next, we further investigate the number of positive equilibria of subsystem S_2 through numerical simulations.

The function $y = M_1(x)$ intersects the x-axis at the point $\left(K\left(1-\frac{a_1}{r}\right), 0\right)$ and intersects the y-axis at the point $(0, y_0)$, where

$$y_0 = \frac{\sqrt{(\beta(1-n)-\varphi a_1)^2 + 4r\varphi\beta(1-n)} - (\beta(1-n)+\varphi a_1)}{2\varphi\beta(1-n)}.$$

$y = M_2(x)$ is a reciprocal function whose center of symmetry is $\left(\frac{\delta}{(1-n)(c\beta-b\delta)}, \frac{a_2 b}{b\delta-c\beta}\right)$, and its intersection with the y-axis is $E^0_{S_2} = \left(0, \frac{a_2}{\delta}\right)$. Differentiating $M_2(x)$, we obtain

$$M_2'(x) = \frac{a_2 c\beta(1-n)}{[\delta(1+b(1-n)x) - c\beta(1-n)x]^2} > 0.$$

Therefore, $M_2(x)$ is strictly increasing on each interval of its domain.

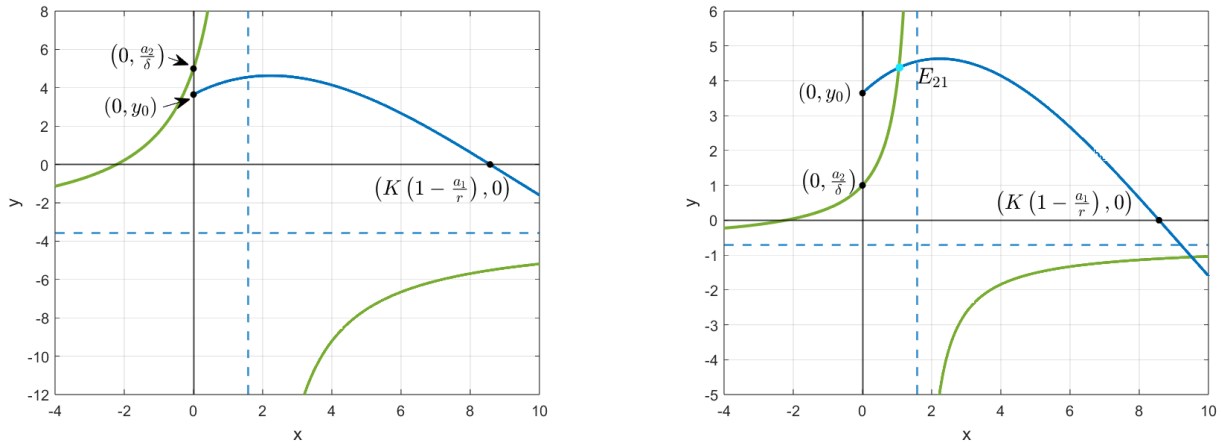

(a) (b)

Figure 1. When $c\beta - b\delta > 0$, the existence of equilibrium points in subsystem S_2. The blue curve represents the pest nullcline, and the green curve represents the natural-enemy nullcline. Parameters are: $r = 1.4$, $\varphi = 0.05$, $K = 10$, $\beta = 0.3$, $n = 0.1$, $b = 0.5$, $c = 0.4$, $\delta = 0.1$, $a_1 = 0.2$, and (a) $a_2 = 0.5$; (b) $a_2 = 0.1$.

When $c\beta - b\delta > 0$, the horizontal asymptote of $M_2(x)$ is $y = \frac{a_2 b}{b\delta - c\beta} < 0$, which lies below the x-axis; its vertical asymptote is $x = \frac{\delta}{(1-n)(c\beta-b\delta)} > 0$, which lies to the right of the y-axis. In this case, the right branch of $M_2(x)$ lies in the fourth quadrant, so in the first quadrant it is only necessary to consider the left branch of $M_2(x)$. When $c\beta - b\delta < 0$, the horizontal asymptote of $M_2(x)$ lies above the x-axis, while

its vertical asymptote lies to the left of the y-axis. In this case, the left branch of $M_2(x)$ lies in the third quadrant, so in the first quadrant it is only necessary to consider the right branch of $M_2(x)$.

(i) When $c\beta - b\delta > 0$, $M_1(x)$ intersects only the left branch of $M_2(x)$ in the first quadrant. If $a_2 < \delta y_0$, then $M_2(x)$ and $M_1(x)$ have one intersection point in first quadrant, as shown in Figure 1(b), denoted by E_{21}. If $a_2 > \delta y_0$, then there is no intersection point, as shown in Figure 1(a). When $a_2 = \delta y_0$, the two nullclines intersect at $E^0_{S_2} = \left(0, \frac{a_2}{\delta}\right)$, at which the boundary equilibrium is a degenerate boundary equilibrium.

(ii) When $c\beta - b\delta < 0$, since $x^*_{S_1} = \frac{\delta}{(1-n)(c\beta - b\delta)} < 0$, subsystem S_1 has no interior equilibrium point. For subsystem S_2, the curves $M_1(x)$ and $M_2(x)$ may have two, one, or no intersections in the first quadrant. When two intersections exist, as shown in Figure 2(a), they are denoted by E^*_{21} and E^*_{22}. When there is only one intersection, as shown in Figure 2(b), it is denoted by E^*_{21}. When no intersection exists, as shown in Figure 2(c), subsystem S_2 admits no interior equilibrium point.

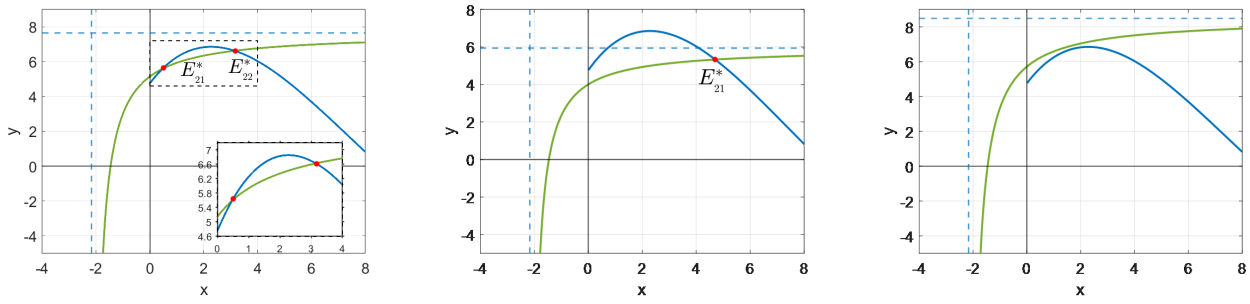

(a) (b) (c)

Figure 2. When $c\beta - b\delta < 0$, the existence of equilibrium points in subsystem S_2. Parameters are: $r = 1.4$, $\varphi = 0.05$, $K = 10$, $\beta = 0.2$, $n = 0.02$, $b = 0.7$, $c = 0.4$, $\delta = 0.35$, $a_1 = 0.2$, and (a) $a_2 = 1.8$; (b) $a_2 = 1.4$; (c) $a_2 = 2$.

The local stability of the equilibria obtained above is then analyzed. The Jacobian matrix is calculated as follows:

$$J(x,y) = \begin{pmatrix} \dfrac{r}{1+\varphi y} - \dfrac{2rx}{K} - \dfrac{\beta(1-n)y}{(1+b(1-n)x)^2} - a_1 & -\dfrac{r\varphi x}{(1+\varphi y)^2} - \dfrac{\beta(1-n)x}{1+b(1-n)x} \\ \dfrac{c\beta(1-n)y}{(1+b(1-n)x)^2} & \dfrac{c\beta(1-n)x}{1+b(1-n)x} - \delta \end{pmatrix}.$$

Substituting the above equilibria into the Jacobian matrix, we can establish the following results:

(i) For the boundary equilibrium point $E^0_{S_2} = \left(0, \frac{a_2}{\delta}\right)$, the eigenvalues of $J\left(E^0_{S_2}\right)$ are $\lambda_1 = \frac{r\delta}{\delta + \varphi a_2} - \frac{\beta(1-n)a_2}{\delta} - a_1$ and $\lambda_2 = -\delta$. When $r\delta < (\delta + \varphi a_2)\left(a_1 + \frac{\beta(1-n)a_2}{\delta}\right)$, the equilibrium point $E^0_{S_2}$ is locally asymptotically stable.

(ii) For the interior equilibrium point $E^*_{S_2} = (x^*, y^*)$, the Jacobian matrix is given by

$$J_{E^*_{S_2}} = \begin{pmatrix} F_x & F_y \\ G_x & G_y \end{pmatrix}\Bigg|_{(x^*, y^*)}.$$

From the equilibrium condition, we obtain

$$F_x(E^*_{S_2}) = -\frac{rx^*}{K} + \frac{b\beta(1-n)^2x^*y^*}{(1+b(1-n)x^*)^2}, \quad F_y(E^*_{S_2}) < 0, \quad G_x(E^*_{S_2}) > 0, \quad G_y(E^*_{S_2}) = -\frac{a_2}{y^*} < 0.$$

Therefore, we have

$$\mathrm{tr}(J_{E^*_{S_2}}) = x^*\left[\frac{\beta b(1-n)^2 y^*}{\left(1+b(1-n)x^*\right)^2} - \frac{r}{K}\right] - \frac{a_2}{y^*},$$

$$\det(J_{E^*_{S_2}}) = -\frac{a_2 x^*}{y^*}\left[\frac{\beta b(1-n)^2 y^*}{\left(1+b(1-n)x^*\right)^2} - \frac{r}{K}\right] + \frac{c\beta(1-n)x^* y^*}{\left(1+b(1-n)x^*\right)^2}\left[\frac{r\varphi}{(1+\varphi y^*)^2} + \frac{\beta(1-n)}{1+b(1-n)x^*}\right].$$

By the stability criterion, $E^*_{S_2}$ is locally asymptotically stable when $\mathrm{tr}(J_{E^*_{S_2}}) < 0$ and $\det(J_{E^*_{S_2}}) > 0$.

Combining the preceding nullcline analysis with the local stability results, we obtain the following conclusions.

Lemma 5. *For the boundary equilibrium $E^0_{S_2} = \left(0, \frac{a_2}{\delta}\right)$, it is unstable if $a_2 < \delta y_0$, and locally asymptotically stable if $a_2 > \delta y_0$.*

Proof. The eigenvalues of the Jacobian matrix at $E^0_{S_2}$ are $\lambda_1 = \frac{r}{1+\phi a_2/\delta} - \frac{\beta(1-n)a_2}{\delta} - a_1$ and $\lambda_2 = -\delta < 0$. Since y_0 satisfies $\frac{r}{1+\phi y_0} - \beta(1-n)y_0 - a_1 = 0$, and

$$\frac{\mathrm{d}}{\mathrm{d}y}\left(\frac{r}{1+\phi y} - \beta(1-n)y - a_1\right) = -\frac{r\phi}{(1+\phi y)^2} - \beta(1-n) < 0,$$

the function $\frac{r}{1+\phi y} - \beta(1-n)y - a_1$ is strictly decreasing with respect to y. Therefore, $\lambda_1 > 0 \iff \frac{a_2}{\delta} < y_0 \iff a_2 < \delta y_0$, whereas $\lambda_1 < 0 \iff \frac{a_2}{\delta} > y_0 \iff a_2 > \delta y_0$. Since $\lambda_2 < 0$, the conclusion follows. □

Theorem 1. *Suppose that $c\beta - b\delta > 0$. If the boundary equilibrium $E^0_{S_2}$ is unstable, then subsystem S_2 admits a unique interior equilibrium. If $E^0_{S_2}$ is locally asymptotically stable, then subsystem S_2 admits no interior equilibrium.*

Proof. By Lemma 5, $E^0_{S_2}$ is unstable if and only if $a_2 < \delta y_0$. In this case, $M_1(0) = y_0 > M_2(0) = \frac{a_2}{\delta}$. Together with the intersection classification established above, this implies that the two nullclines have a unique intersection in the first quadrant. If $a_2 > \delta y_0$, then $M_1(0) < M_2(0)$, and the preceding nullcline analysis shows that no intersection exists. □

Theorem 2. *Suppose that $c\beta - b\delta < 0$. If $E^0_{S_2}$ is unstable, then subsystem S_2 admits a unique interior equilibrium. If $E^0_{S_2}$ is locally asymptotically stable, then subsystem S_2 may admit two interior equilibria or no interior equilibrium. At the critical tangency condition, subsystem S_2 admits one interior equilibrium.*

Proof. Let $\bar{x} = K\left(1 - \frac{a_1}{r}\right)$. Since $M_1(0) = y_0$, $M_2(0) = \frac{a_2}{\delta}$, Lemma 5 implies that, when $E^0_{S_2}$ is unstable, $M_1(0) > M_2(0)$. Moreover, $M_1(\bar{x}) = 0 < M_2(\bar{x})$. Thus, the relative positions of the two nullclines at the two endpoints are opposite. By classification of the nullcline configurations shown, $M_1(x)$ and $M_2(x)$ have a unique intersection in the first quadrant.

When $E^0_{S_2}$ is locally asymptotically stable, Lemma 5 gives $M_1(0) < M_2(0)$, while $M_1(\bar{x}) < M_2(\bar{x})$ still holds. Hence, the two nullclines have the same relative positions at both endpoints. Depending on their relative positions in the interior of $(0, \bar{x})$, they may intersect twice or have no intersection. At the critical parameter value, the two nullclines are tangent and have one intersection. □

Next, we further investigate the local stability of the equilibrium points of the subsystem S_2 through numerical simulations, and the results are shown in Figure 3. When $c\beta - b\delta > 0$, as shown in Figure 3(a), subsystem S_2 has one positive equilibrium point E_{21}, which is a stable focus. When $c\beta - b\delta < 0$, different dynamical scenarios may occur as a_2 varies. For Figure 3(b), the boundary equilibrium point $E^0_{S_2}$ is a stable node, E^*_{21} is a saddle point, and E^*_{22} is a stable focus. For Figure 3(c), $E^0_{S_2}$ is unstable, and E^*_{21} is a stable node.

From a biological perspective, the stability of $E^0_{S_2} = (0, \frac{a_2}{\delta})$ indicates that pesticide application and natural enemy release can eliminate the pest population, while the natural enemy population is maintained by continuous release. The instability of $E^0_{S_2}$ means that the pest population cannot be eliminated and may persist in the system. Moreover, the stability of the positive equilibrium indicates that pests and natural enemies can coexist under the combined effects of natural predation and pest-control measures. If the equilibrium pest density is below the economic threshold ET, the control strategy is considered effective. Otherwise, stronger or more frequent control measures may be required.

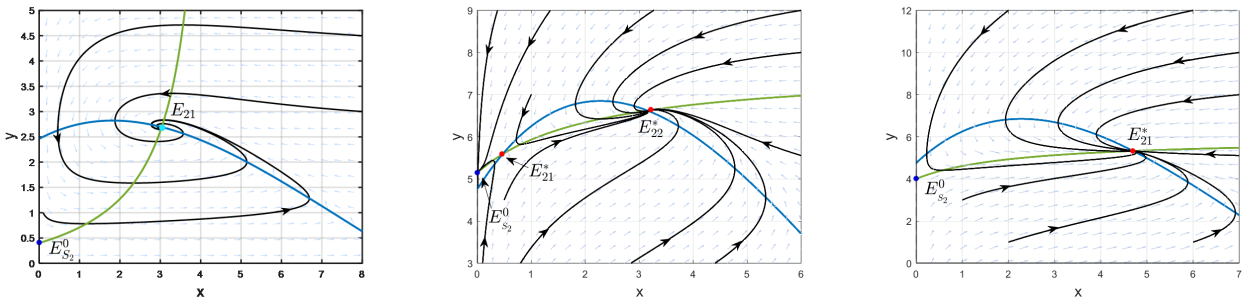

(a) (b) (c)

Figure 3. Phase portraits of subsystem S_2 under different parameter values. Parameters are: (a) $r = 1.4$, $\varphi = 0.05$, $K = 10$, $\beta = 0.5$, $n = 0.25$, $b = 0.5$, $c = 0.4$, $\delta = 0.25$, $a_1 = 0.2$, and $a_2 = 0.1$; (b) $r = 1.4$, $\varphi = 0.05$, $K = 10$, $\beta = 0.2$, $n = 0.02$, $b = 0.7$, $c = 0.4$, $\delta = 0.35$, $a_1 = 0.2$, and $a_2 = 1.8$; (c) same as in (b), except that $a_2 = 1.4$.

4. Sliding dynamics

4.1. Sliding region

Let

$$\sigma(Z) = \langle \nabla H_Z, F_{G_1}(Z) \rangle \langle \nabla H_Z, F_{G_2}(Z) \rangle,$$

where $\langle \cdot, \cdot \rangle$ denotes the standard scalar product. According to the Filippov convention adopted in this paper, the switching manifold is divided into the following regions:

(a) **Crossing region:** $\Sigma_c = \{Z \in \Sigma \mid \sigma(Z) > 0\}$.
(b) **Attracting sliding region:** $\Sigma_{as} = \{Z \in \Sigma \,\big|\, \langle \nabla H_Z, F_{G_1}(Z) \rangle \geq 0, \langle \nabla H_Z, F_{G_2}(Z) \rangle \leq 0\}$.
(c) **Escaping region:** $\Sigma_{es} = \{Z \in \Sigma \,\big|\, \langle \nabla H_Z, F_{G_1}(Z) \rangle < 0, \langle \nabla H_Z, F_{G_2}(Z) \rangle > 0\}$.

The sliding region, denoted by Σ_s, consists of the attracting sliding region Σ_{as} and the escaping sliding region Σ_{es}, namely, $\Sigma_s = \Sigma_{as} \cup \Sigma_{es}$.

We next discuss the different regions on the switching manifold Σ. Setting $\langle \nabla H_Z, F_{G_1}(Z)\rangle = 0$ and simplifying, we obtain

$$T_1(y) = A_1 y^2 + B_1 y + C_1 = 0,$$

where $A_1 = K\varphi\beta(1-n) > 0$, $B_1 = K\beta(1-n) + \varphi rET(1 + b(1-n)ET) > 0$, and $C_1 = r(1 + b(1-n)ET)(ET - K)$.

If $ET < K$, then $C_1 < 0$, and hence the equation $T_1(y) = 0$ has a unique positive root, namely

$$y_{c_1} = \frac{\sqrt{\Delta_1} - K\beta(1-n) - \varphi rET(1 + b(1-n)ET)}{2K\varphi\beta(1-n)},$$

where

$$\Delta_1 = \left[K\beta(1-n) - \varphi rET(1 + b(1-n)ET)\right]^2 + 4K^2 r\varphi\beta(1-n)(1 + b(1-n)ET).$$

Setting $\langle \nabla H_Z, F_{G_2}\rangle = 0$ and simplifying, we obtain

$$T_2(y) = A_2 y^2 + B_2 y + C_2 = 0,$$

where $A_2 = K\varphi\beta(1-n) > 0$, $B_2 = K\beta(1-n) + \varphi(1 + b(1-n)ET)(rET + Ka_1) > 0$, and $C_2 = (1 + b(1-n)ET)(rET + Ka_1 - Kr)$.

If $ET < K\left(1 - \frac{a_1}{r}\right)$, then $C_2 < 0$, and hence the equation $T_2(y) = 0$ has a unique positive root, namely

$$y_{c2} = \frac{\sqrt{\Delta_2} - K\beta(1-n) - \varphi(1 + b(1-n)ET)(rET + Ka_1)}{2K\varphi\beta(1-n)},$$

where

$$\Delta_2 = \left[K\beta(1-n) - \varphi(1 + b(1-n)ET)(rET + Ka_1)\right]^2 + 4K^2 r\varphi\beta(1-n)(1 + b(1-n)ET).$$

When $\langle \nabla H_Z, F_{G_1}\rangle \geq 0, \langle \nabla H_Z, F_{G_2}\rangle \leq 0$, that is, $T_1(y) \leq 0$ and $T_2(y) \geq 0$, the system admits an attracting sliding region on the switching manifold. Depending on the value of ET, the attracting sliding and crossing regions can be classified into the following three cases.

(i) When $ET < K\left(1 - \frac{a_1}{r}\right)$, the equations $T_1(y) = 0$ and $T_2(y) = 0$ each have a unique positive root, denoted by y_{c1} and y_{c2}, respectively, with $y_{c2} \leq y_{c1}$. Hence, the attracting sliding region is $\Sigma_{as} = \left\{(x,y)^T \in \Sigma : \ y_{c2} \leq y \leq y_{c1}\right\}$, while the crossing region is $\Sigma_c = \left\{(x,y)^T \in \Sigma : \ 0 < y < y_{c2}\right\} \cup \left\{(x,y)^T \in \Sigma : \ y > y_{c1}\right\}$.

(ii) When $K\left(1 - \frac{a_1}{r}\right) < ET < K$, the equation $T_1(y) = 0$ has a unique positive root y_{c1}, whereas $T_2(y) = 0$ has no positive root. Therefore, the attracting sliding region is $\Sigma_{as} = \left\{(x,y)^T \in \Sigma : \ 0 < y \leq y_{c1}\right\}$, while the crossing region is $\Sigma_c = \left\{(x,y)^T \in \Sigma : \ y > y_{c1}\right\}$.

(iii) When $ET > K$, for any $y > 0$, one has $\langle \nabla H_Z, F_{G_1}\rangle < 0$, $\langle \nabla H_Z, F_{G_2}\rangle < 0$. Therefore, the crossing region is $\Sigma_c = \left\{(x,y)^T \in \Sigma : \ y > 0\right\}$, and no attracting sliding mode exists on the switching manifold Σ.

Furthermore, according to the Filippov convention adopted in this paper, if an escaping region exists on the switching surface, it must satisfy $\langle \nabla H_Z, F_{G_1}\rangle < 0$, $\langle \nabla H_Z, F_{G_2}\rangle > 0$. This implies that $\langle \nabla H_Z, F_{G_1}\rangle - \langle \nabla H_Z, F_{G_2}\rangle < 0$. However, direct calculation yields $\langle \nabla H_Z, F_{G_1}\rangle - \langle \nabla H_Z, F_{G_2}\rangle = a_1 ET > 0$. The two results contradict each other. Therefore, no escaping region exists in the Filippov system.

The above classification of the sliding regions provides further insights into the biological implications of different economic thresholds.

(i) If $ET < K\left(1-\frac{a_1}{r}\right)$, the economic threshold is lower than the pest equilibrium level under pesticide application alone. This indicates that pesticide application alone cannot reduce the pest population to a level below the threshold in the long term. Consequently, after the pest density exceeds the threshold and control measures are activated, the pest population may remain around the threshold due to the combined effects of pesticide application, natural predation, and pest population growth, resulting in possible sliding motion caused by repeated switching between the two subsystems.

(ii) If $K\left(1-\frac{a_1}{r}\right) < ET < K$, the threshold lies between the pest equilibrium level under pesticide control alone and the environmental carrying capacity. In this case, without control measures, the pest population can naturally increase and reach the economic threshold. Once the threshold is exceeded, pesticide application and natural enemy release are activated, which suppress the pest population and drive it back toward the threshold region, thereby generating an attracting sliding regime near ET.

(iii) If $ET > K$, the threshold exceeds the environmental carrying capacity. Therefore, the pest population cannot reach the switching boundary from below, and the threshold-based control strategy is unlikely to be activated. Consequently, no attracting sliding mode exists.

4.2. Equilibria of the Filippov system

In this section, five types of equilibrium points of the Filippov system (2.4) are discussed.

Pseudo-equilibrium: We adopt Utkin's equivalent control method to study the nonsmooth dynamical behavior. On the sliding surface, We define the system's convex combination:

$$\begin{pmatrix} \dfrac{dx}{dt} \\ \dfrac{dy}{dt} \end{pmatrix} = \lambda F_{G_1} + (1-\lambda) F_{G_2}, \tag{4.1}$$

where

$$\lambda = \frac{\langle F_{G_2}, \nabla H_Z \rangle}{\langle F_{G_2}, \nabla H_Z \rangle - \langle F_{G_1}, \nabla H_Z \rangle}.$$

After direct computation, we obtain:

$$\lambda = -\frac{rx\left(\frac{1}{1+\varphi y}-\frac{x}{K}\right)-\frac{\beta(1-n)xy}{1+b(1-n)x}-a_1x}{a_1x} = 1+\frac{1}{a_1}\left(\frac{\beta(1-n)y}{1+b(1-n)x}+\frac{rx}{K}-\frac{r}{1+\varphi y}\right).$$

Let $x = ET$. Substituting the expression of λ into Eq (4.1), we obtain:

$$\begin{cases} \dfrac{dx}{dt} = 0, \\ \dfrac{dy}{dt} = \dfrac{c\beta(1-n)ET\,y}{1+b(1-n)ET} - \delta y + \dfrac{a_2}{a_1}\left[r\left(\dfrac{1}{1+\varphi y}-\dfrac{ET}{K}\right)-\dfrac{\beta(1-n)y}{1+b(1-n)ET}\right]. \end{cases}$$

Setting the sliding-mode dynamics equal to zero and simplifying, we obtain:

$$\frac{dy}{dt} = -\frac{1}{Ka_1(1+\varphi y)(1+b(1-n)ET)}\, g_1(y) = 0,$$

where

$$g_1(y) = A_3y^2 + B_3y + C_3,$$

with

$$A_3 = K\varphi a_1(1-n)(b\delta ET - \beta cET) + K\varphi a_2\beta(1-n) + K\varphi a_1\delta,$$
$$B_3 = ba_2\varphi r(1-n)ET^2 + Ka_1(1-n)(b\delta - \beta c)ET + K(1-n)a_2\beta + Ka_1\delta + a_2\varphi rET$$
$$= ba_2\varphi r(1-n)ET^2 + \frac{A_3}{\varphi} + a_2\varphi rET,$$
$$C_3 = -a_2r(K-ET)(bET(1-n)+1) < 0.$$

Here, we only consider the case $\Delta_3 = B_3^2 - 4A_3C_3 > 0$. When $\Delta_3 > 0$, this equation has two distinct real roots, denoted by y_{p_1} and y_{p_2}, given by

$$y_{p_1} = \frac{-B_3 + \sqrt{\Delta_3}}{2A_3}, \qquad y_{p_2} = \frac{-B_3 - \sqrt{\Delta_3}}{2A_3}.$$

Combining the polynomial $g_1(y)$ with the parameters A_3, B_3, and C_3 defined above, the number of positive roots can be classified into the following three cases:

(i) If $A_3 > 0$, then $B_3 > 0$. Since $C_3 < 0$, we have $y_{p_1}y_{p_2} = \frac{C_3}{A_3} < 0$. Hence, $y_{p_1} > 0, y_{p_2} < 0$.

(ii) If $A_3 < 0$ and $B_3 > 0$, then, since $C_3 < 0$, we have $y_{p_1}y_{p_2} = \frac{C_3}{A_3} > 0, y_{p_1} + y_{p_2} = -\frac{B_3}{A_3} > 0$. Hence, $y_{p_1} > 0, y_{p_2} > 0$.

(iii) If $A_3 < 0$ and $B_3 < 0$, then, since $C_3 < 0$, we have $y_{p_1}y_{p_2} = \frac{C_3}{A_3} > 0, y_{p_1} + y_{p_2} = -\frac{B_3}{A_3} < 0$. Hence, $y_{p_1} < 0, y_{p_2} < 0$.

Furthermore, if a positive root y_{p_i} $(i = 1, 2)$ lies in the interior of the sliding region, that is, $y_{c2} < y_{p_i} < y_{c1}$, and the corresponding convex coefficient satisfies $0 < \lambda(E_{p_i}) < 1$, then $E_{p_i} = (ET, y_{p_i})$ is a pseudo-equilibrium of system (2.4).

Next, we analyze the stability of the pseudo-equilibria. Let

$$\frac{dy}{dt} = F(y) = -\frac{g_1(y)}{Ka_1(1+\varphi y)(1+b(1-n)ET)},$$

then

$$F'(y) = -\frac{1}{Ka_1(1+b(1-n)ET)}\left(\frac{(1+\varphi y)(2A_3y + B_3) - \varphi(A_3y^2 + B_3y + C_3)}{(1+\varphi y)^2}\right). \tag{4.2}$$

Substituting y_{p_1} and y_{p_2} into Eq (4.2), we obtain

$$F'(y_{p_1}) = -\frac{\sqrt{\Delta_3}}{Ka_1(1+b(1-n)ET)(1+\varphi y_{p_1})} < 0,$$

and

$$F'(y_{p_2}) = \frac{\sqrt{\Delta_3}}{Ka_1(1+b(1-n)ET)(1+\varphi y_{p_2})} > 0.$$

Combining existence conditions with the stability analysis, we conclude that E_{p_1} is a locally asymptotically stable pseudo-node in its admissible parameter region, whereas E_{p_2} is a pseudo-saddle.

Tangency points: In the Filippov system, the tangency points satisfy:

$$\begin{cases} \dfrac{dx}{dt} = \dfrac{rx}{1+\varphi y} - \dfrac{rx^2}{K} - \dfrac{\beta(1-n)xy}{1+b(1-n)x}, \\ x = ET, \end{cases} \quad \text{or} \quad \begin{cases} \dfrac{dx}{dt} = \dfrac{rx}{1+\varphi y} - \dfrac{rx^2}{K} - \dfrac{\beta(1-n)xy}{1+b(1-n)x} - a_1x, \\ x = ET. \end{cases}$$

Hence, the tangency points are $T_1(ET, y_{c1}), T_2(ET, y_{c2})$.

Boundary equilibrium: The two boundary equilibrium points associated with the Filippov system are determined by the following equations:

$$\begin{cases} \dfrac{dx}{dt} = \dfrac{rx}{1+\varphi y} - \dfrac{rx^2}{K} - \dfrac{\beta(1-n)xy}{1+b(1-n)x}, \\ \dfrac{dy}{dt} = \dfrac{c\beta(1-n)xy}{1+b(1-n)x} - \delta y, \\ x = ET, \end{cases} \quad \text{or} \quad \begin{cases} \dfrac{dx}{dt} = \dfrac{rx}{1+\varphi y} - \dfrac{rx^2}{K} - \dfrac{\beta(1-n)xy}{1+b(1-n)x} - a_1 x, \\ \dfrac{dy}{dt} = \dfrac{c\beta(1-n)xy}{1+b(1-n)x} - \delta y + a_2, \\ x = ET. \end{cases}$$

The Filippov system admits two boundary equilibria $E_B^1(ET, y_{c1})$ and $E_B^2(ET, y_{c2})$.

When $ET = \frac{\delta}{(1-n)(c\beta - b\delta)}$, the tangency point T_1 coincides with E_B^1. Moreover, when $y_{c2} = \frac{a_2(1+b(1-n)ET)}{\delta(1+b(1-n)ET) - c\beta(1-n)ET}$, the tangency point T_2 coincides with E_B^2.

Regular equilibria: When $c\beta - b\delta > 0$, the subsystems S_1 and S_2 admit unique interior equilibrium points $E^*_{S_1} = (x_1, y_1)$ and $E^*_{S_2} = (x_2, y_2)$, respectively, with $x_1 > x_2$. When $c\beta - b\delta < 0$, the subsystem S_1 has a locally asymptotically stable boundary equilibrium point $E^0_{S_1} = (K, 0)$. As shown in Figure 3(b), the subsystem S_2 has two interior equilibrium points $E^*_{21} = (x^*_{21}, y^*_{21})$ and $E^*_{22} = (x^*_{22}, y^*_{22})$. The classification of the equilibria under different parameter and threshold conditions is summarized in Table 1, where the subscripts (R) and (V) denote real and virtual equilibria, respectively.

Table 1. Classification of equilibria under different parameter and threshold conditions.

Parameter condition	Threshold condition	Equilibrium configuration
$c\beta - b\delta > 0$	$x_2 < x_1 < ET$	$E_R^1 = E^*_{S_1}, \quad E_V^2 = E^*_{S_2}$
	$x_2 < ET < x_1$	$E_V^1 = E^*_{S_1}, \quad E_V^2 = E^*_{S_2}$
	$ET < x_2 < x_1$	$E_V^1 = E^*_{S_1}, \quad E_R^2 = E^*_{S_2}$
$c\beta - b\delta < 0$	$K < ET$	$E_R^{10} = E^0_{S_1}, \quad E_V^{21} = E^*_{21}, \quad E_V^{22} = E^*_{22}$
	$x^*_{22} < ET < K$	$E_V^{10} = E^0_{S_1}, \quad E_V^{21} = E^*_{21}, \quad E_V^{22} = E^*_{22}$
	$x^*_{21} < ET < x^*_{22}$	$E_V^{10} = E^0_{S_1}, \quad E_V^{21} = E^*_{21}, \quad E_R^{22} = E^*_{22}$
	$ET < x^*_{21} < x^*_{22}$	$E_V^{10} = E^0_{S_1}, \quad E_R^{21} = E^*_{21}, \quad E_R^{22} = E^*_{22}$

In particular, when $x_2 < ET < x_1$ or $x^*_{21} < ET < x^*_{22}$, the following conclusions hold:

(i) If $A_3 > 0, B_3 > 0, C_3 < 0$, and $y_{c2} < y_{p_1} < y_{c1}$, then the system admits a pseudo-equilibrium E_{p_1}.
(ii) If $A_3 < 0, B_3 > 0, C_3 < 0$, and $y_{c2} < y_{p_i} < y_{c1}$ $(i = 1, 2)$, then the system admits both pseudo-equilibria E_{p_1} and E_{p_2}.

To further illustrate the role of economic threshold ET in the system (2.4), Figure 4 presents a bifurcation diagram of the system with respect to ET for a given set of parameters. In Figure 4, the blue and cyan curves represent the tangent curves $T_1(y)$ and $T_2(y)$ of subsystems S_1 and S_2, respectively; the black dashed curves denote the branches of the interior equilibria of S_1 and S_2; the green curve represents the roots of the sliding mode equation $g_1(y) = 0$; and the red curve indicates the existence interval of the pseudo-equilibrium point E_{p_1}. It can be seen that the sliding segment Σ_s is bounded by $T_1(y)$ and $T_2(y)$. When the branch of the interior equilibrium point $E^*_{S_2}$ of subsystem S_2 intersects the

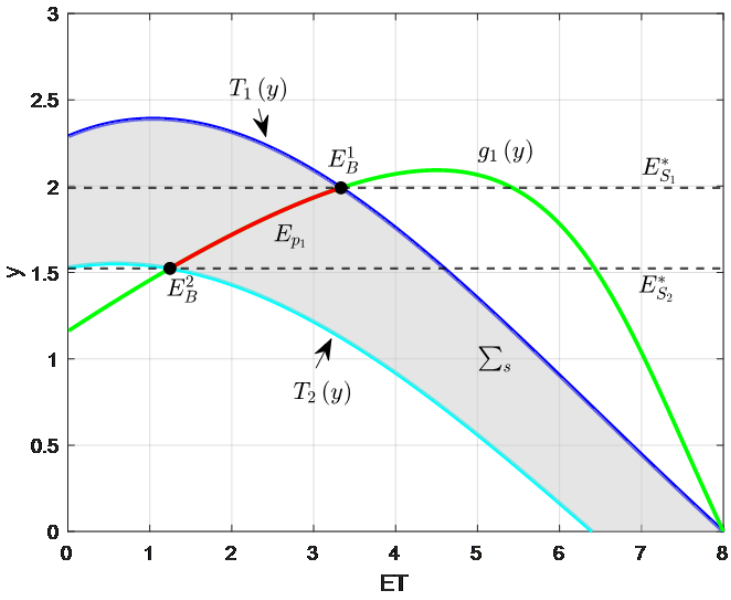

Figure 4. Bifurcation diagram of different types of equilibria of system (2.4) with respect to ET. Parameters are: $r = 1$, $\varphi = 0.2$, $K = 8$, $\beta = 0.5$, $n = 0.4$, $b = 0.5$, $c = 0.4$, $\delta = 0.2$, $a_1 = 0.2$, and $a_2 = 0.1$.

curve $g_1(y) = 0$ at a certain critical threshold, the boundary equilibrium point E_B^2 emerges, and a stable pseudo-equilibrium point E_{p_1} appears in the sliding mode. As economic threshold ET increases, when the interior equilibrium point $E_{S_1}^*$ intersects the curve $g_1(y) = 0$ at $ET = 3.3$, the boundary equilibrium point E_B^1 appears, and the pseudo-equilibrium point E_{p_1} disappears.

5. Sliding bifurcation analysis

5.1. Sliding bifurcations

In the Filippov system, the emergence of a sliding segment may induce sliding bifurcations, thereby affecting pest-control outcomes. The pesticide-induced per capita mortality rate a_1, the constant natural-enemy release rate a_2, and the refuge coefficient n all affect the effectiveness of pest control. With the remaining parameters fixed, we numerically investigate the effects of these parameters on pest-control outcomes.

As shown in Figure 5(a), when the pesticide-induced per capita mortality rate a_1 is small, the pseudo-equilibrium point E_{p_1} gradually changes from nonexistence to existence as the economic threshold ET increases. Comparing Figure 5(a) and Figure 5(b), it can be seen that, as a_1 increases, the length of the sliding segment also increases. When $a_1 = 0.6$, E_{p_1} consistently exists and is stable on the sliding segment Σ_s. Comparing Figure 5(a) and Figure 5(c), it can be seen that, as a_2 increases, the sliding segment remains invariant, whereas E_{p_1} gradually shifts upward. When a_2 reaches 0.4, E_{p_1} consistently exists and remains stable on the Σ_s.

From the viewpoint of pest management, choosing appropriate insecticide concentration and natural enemy release rate can ensure the existence of a stable pseudo-equilibrium on the sliding segment,

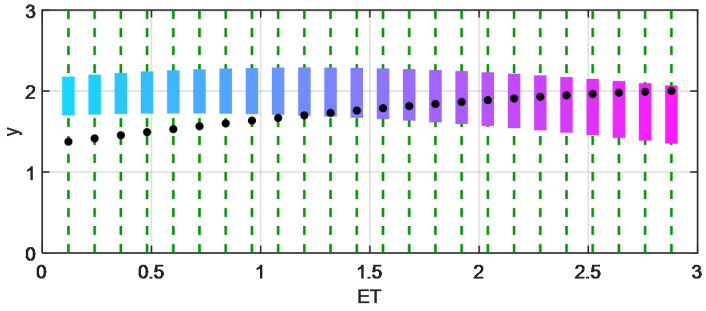

(a) $a_1 = 0.2,\ a_2 = 0.15$

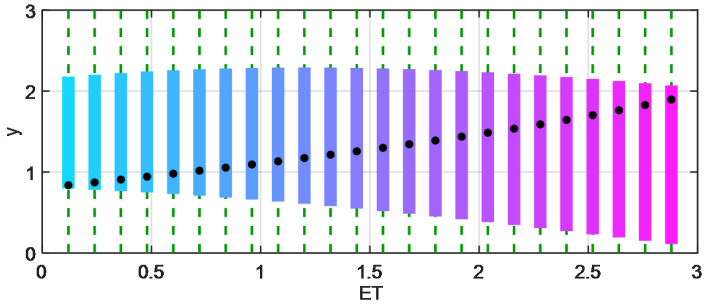

(b) $a_1 = 0.6,\ a_2 = 0.15$

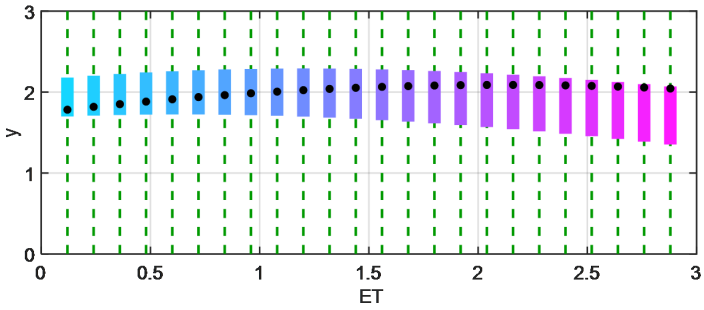

(c) $a_1 = 0.2,\ a_2 = 0.4$

Figure 5. Sliding bifurcation diagrams of system (2.4) with respect to ET, where $ET \in [0, 3]$. Parameters are: $r = 1$, $\varphi = 0.2$, $K = 8$, $\beta = 0.5$, $n = 0.35$, $b = 0.5$, $c = 0.4$, and $\delta = 0.2$. The colored vertical segments represent the attracting sliding regions; the black dots denote the stable pseudo-equilibria.

thereby keeping the pest density within a controllable range.

As shown in Figure 6, when the refuge coefficient n is small, E_{p_1} consistently exists and is stable on the sliding segment Σ_s. As n gradually increases, E_{p_1} gradually moves away from the sliding segment, and the interval in which the pseudo-equilibrium point exists continuously shrinks and may even disappear. This indicates that the refuge behavior of pests weakens the control effects of natural enemies, thereby compromising the overall performance of integrated pest management.

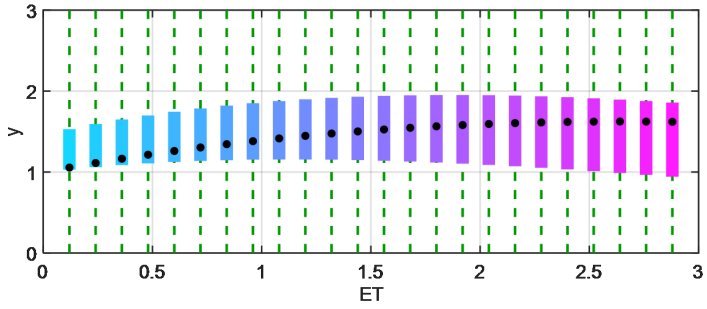

(a) $n = 0.05$

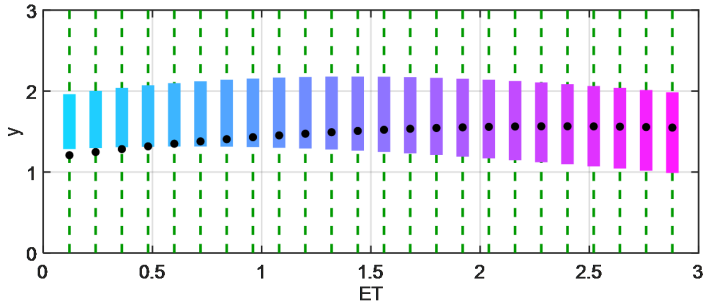

(b) $n = 0.36$

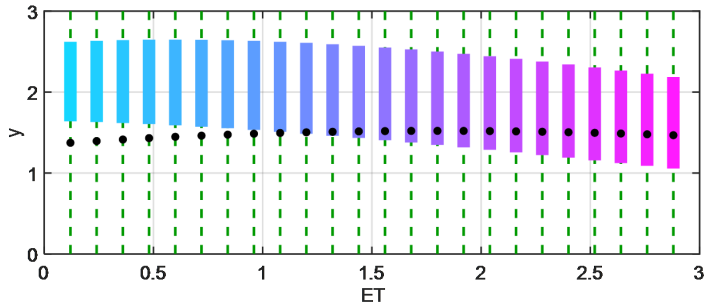

(c) $n = 0.6$

Figure 6. Sliding bifurcation diagrams of system (2.4) with respect to ET. Parameters are: $r = 1.2$, $\varphi = 0.5$, $K = 10$, $\beta = 0.5$, $b = 0.8$, $c = 0.4$, $\delta = 0.2$, $a_1 = 0.33$, and $a_2 = 0.20$. The colored vertical segments represent the attracting sliding regions; the black dots denote the stable pseudo-equilibria.

5.2. Boundary equilibrium bifurcation

When a parameter passes through a critical threshold, a stable node or a stable focus may collide with a tangency point on the discontinuity surface, thereby giving rise to a boundary-node bifurcation or a boundary-focus bifurcation.

Let $E^*_{S_i} = (x^*_i, y^*_i)$ be a regular equilibrium of subsystem S_i. A boundary equilibrium bifurcation may occur when $H(E^*_{S_i}, ET_c) = x^*_i - ET_c = 0$. Since $\frac{\partial H(E^*_{S_i}, ET)}{\partial ET} = -1 \neq 0$, the equilibrium crosses the switching manifold transversally as ET passes through the critical value $ET_c = x^*_i$. The node or focus

type is determined by the eigenvalues of the corresponding Jacobian matrix.

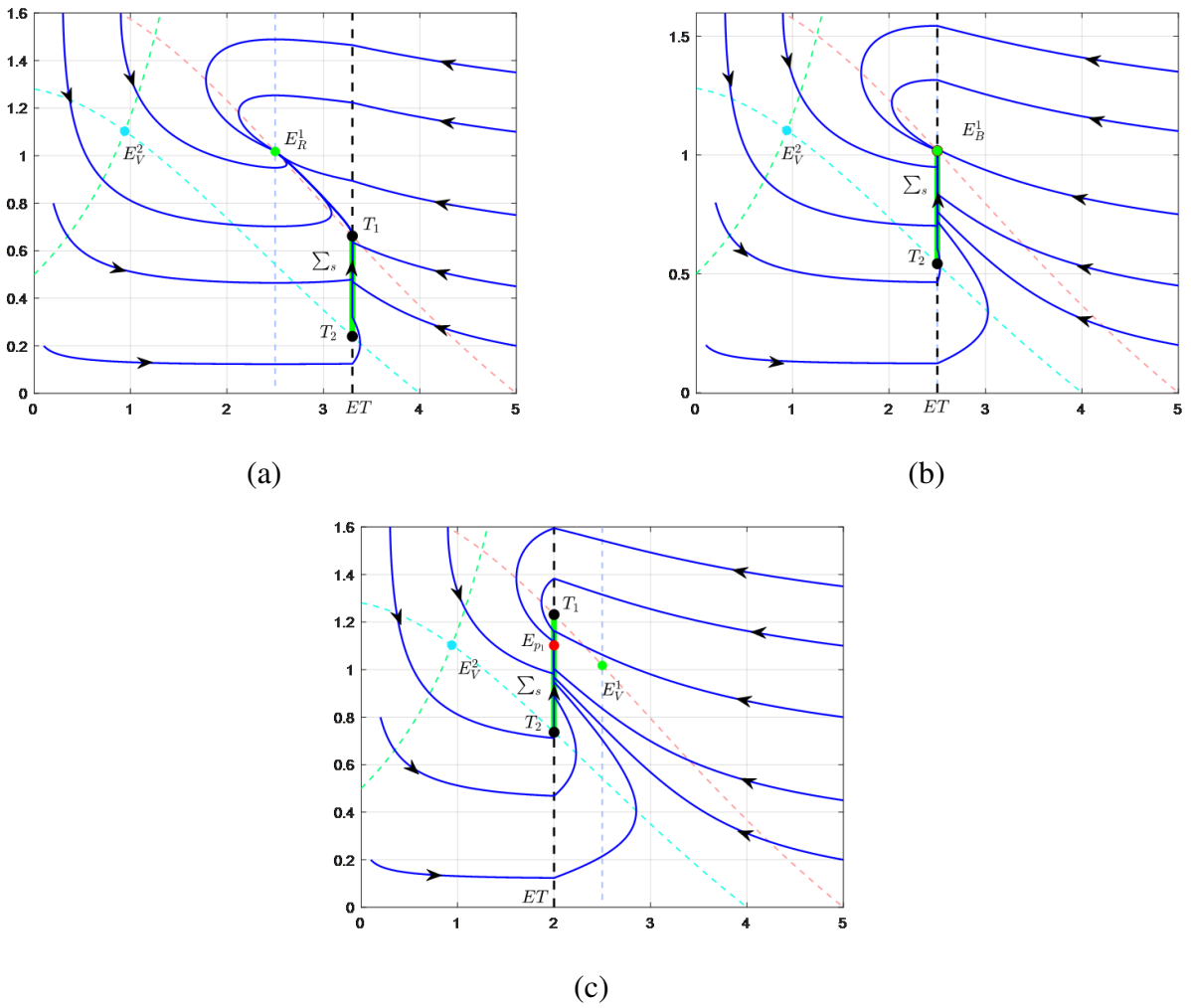

Figure 7. Boundary-node bifurcation of system (2.4). Parameter values: $r = 1$, $\varphi = 0.5$, $K = 5$, $\beta = 0.4$, $n = 0.2$, $b = 0.5$, $c = 0.5$, $\delta = 0.2$, $a_1 = 0.2$, $a_2 = 0.1$, and (a) $ET = 3.3$; (b) $ET = 2.5$; (c) $ET = 2$. As ET decreases, the stable node E_R^1 collides with the tangency point T_1 to form the boundary equilibrium E_B^1, which subsequently bifurcates into the pseudo-equilibrium E_{p_1}, the tangency point T_1, and the virtual equilibrium E_V^1.

Boundary-node bifurcation: For $ET = 3.3$, the stable node E_R^1 lies to the left of the switching boundary $x = ET$, as illustrated in Figure 7(a). Under the current parameter conditions, predation by natural enemies alone is sufficient to control the pest population within a safe range, and no additional control measures are required. The local asymptotic stability of E_R^1 means that, in subsystem S_1, small disturbances in the pest and natural-enemy populations eventually disappear, and the two populations return to a coexistence state maintained by natural predation and the fear effect, without pesticide application or artificial release of natural enemies.

As shown in Figure 7(b), when ET decreases to 2.5, the stable node E_R^1 meets the tangency point T_1, forming the boundary equilibrium point E_B^1. At this time, the pest population has approached the

critical level at which control measures are required, and the system is in a relatively sensitive state: If pest growth increases slightly or the suppressive effect of natural enemies weakens slightly, the pest population may exceed the economic threshold, thereby triggering control measures.

When the economic threshold ET further decreases to 2, the boundary equilibrium point E_B^1 of system (2.4) disappears and is transformed into a pseudo-equilibrium point E_{p_1}, a tangency point T_1, and a virtual equilibrium point E_V^1, as illustrated in Figure 7(c).

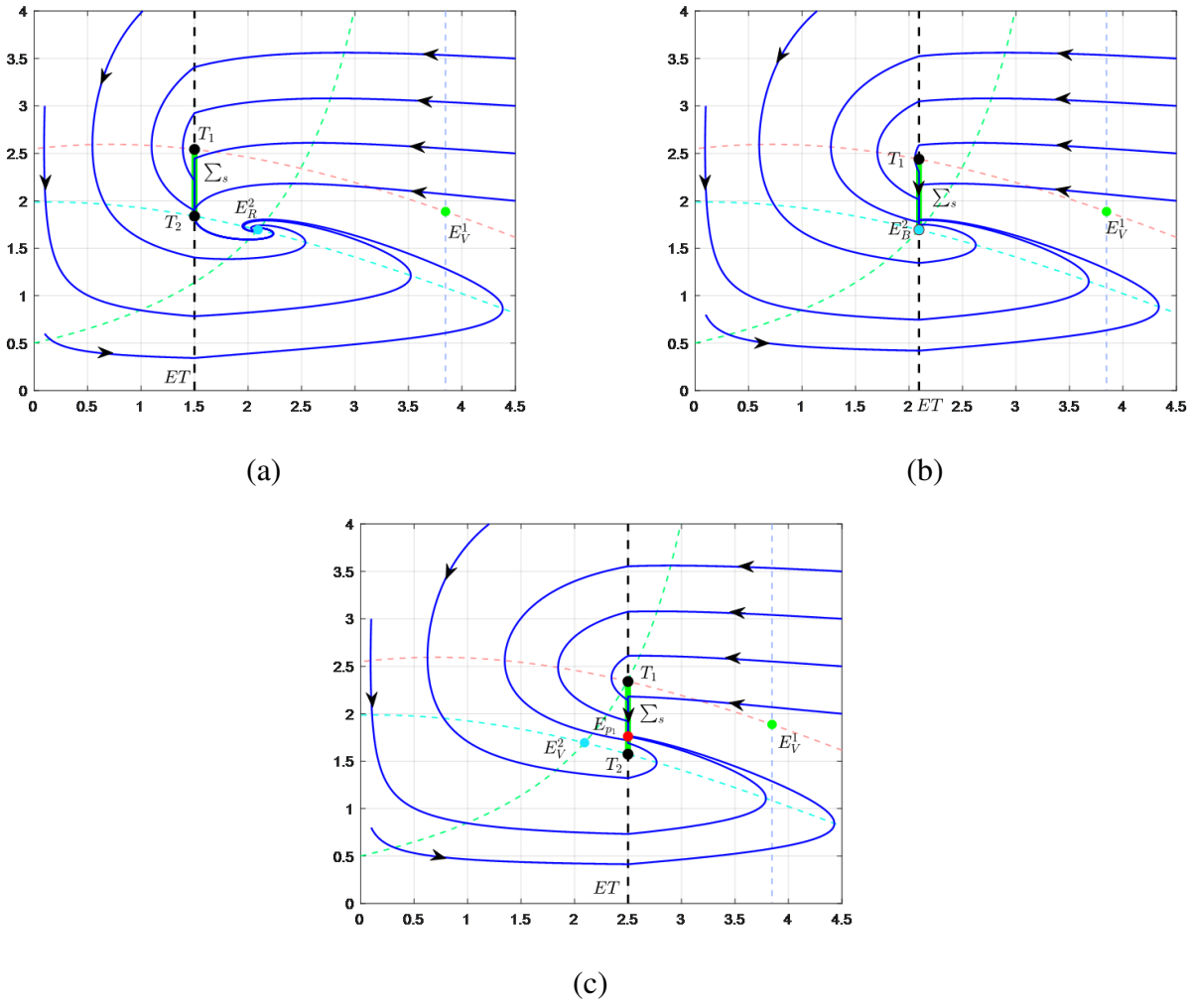

Figure 8. Boundary-focus bifurcation of system (2.4). Parameter values: $r = 1$, $\varphi = 0.2$, $K = 8$, $\beta = 0.5$, $n = 0.48$, $b = 0.5$, $c = 0.4$, $\delta = 0.2$, $a_1 = 0.2$, $a_2 = 0.1$, and (a) $ET = 1.5$; (b) $ET = 2.09$; (c) $ET = 2.5$. As ET increases, the stable focus E_R^2 collides with the tangency point T_2 to form the boundary equilibrium E_B^2, which subsequently bifurcates into the pseudo-equilibrium E_{p_1}, the tangency point T_2, and the virtual equilibrium E_V^2.

Boundary-focus bifurcation: Figure 8 illustrates the boundary-focus bifurcation induced by increasing ET. When $ET = 1.5$, subsystem S_2 possesses a stable focus E_R^2, and the pest and natural enemy populations converge to a stable state in an oscillatory manner. The local asymptotic stability of E_R^2 means that, under subsystem S_2, small population disturbances eventually decay and the pest

and natural-enemy populations return to a coexistence state maintained by the combined effects of pesticide application, natural predation, the fear effect, and continuous release of natural enemies. When the economic threshold ET increases to 2.09, the stable focus E_R^2 coincides with the tangency point T_2, giving rise to the boundary equilibrium point E_B^2, and the system enters a critical control state. When the economic threshold ET further increases to 2.5, the boundary equilibrium point E_B^2 disappears and is replaced by a stable pseudo-equilibrium point E_{p_1}, a tangency point T_2, and a virtual equilibrium point E_V^2. Consequently, the pest density is eventually controlled near the economic threshold.

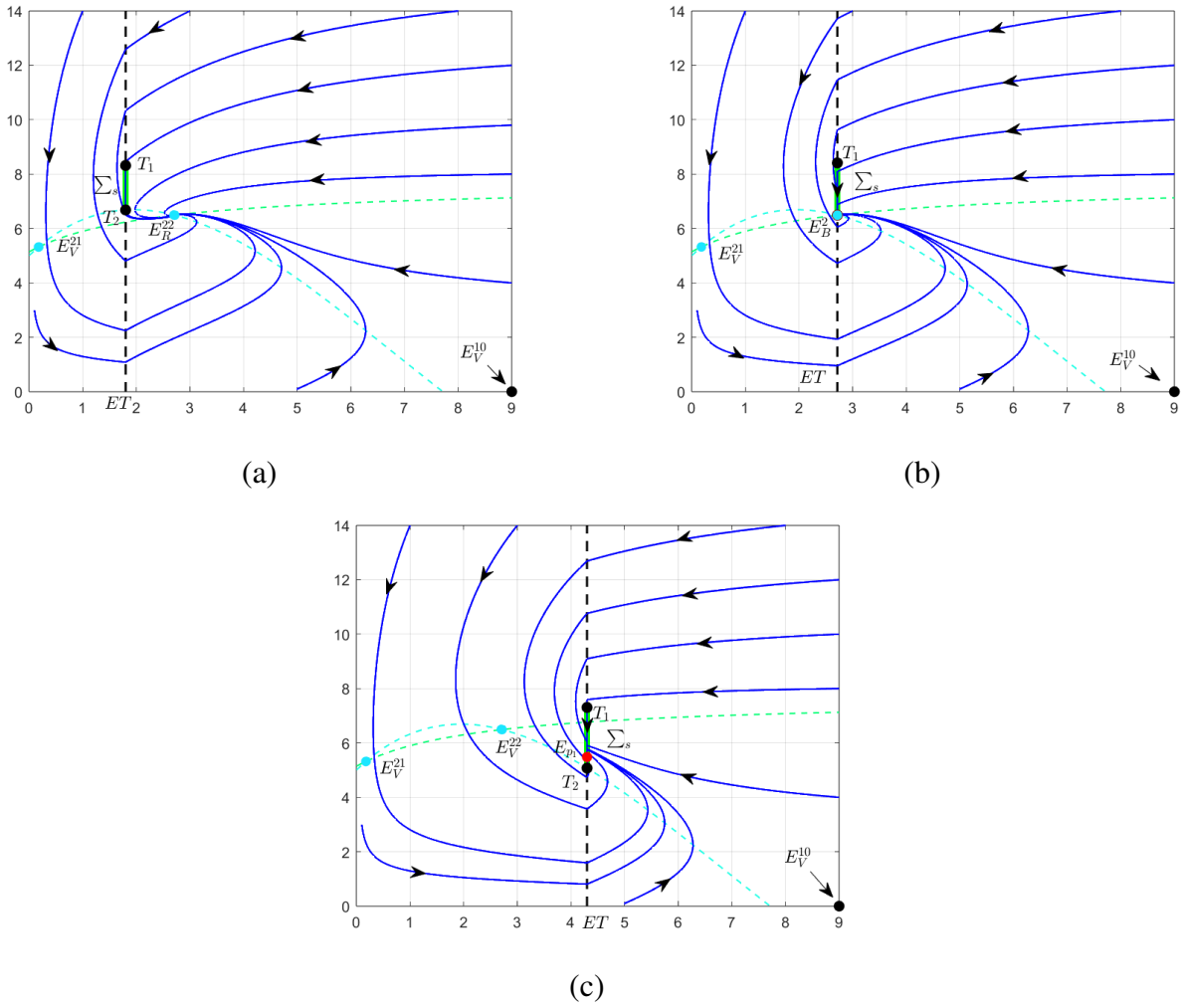

Figure 9. Another boundary-focus bifurcation of system (2.4). Parameter values: $r = 1.4$, $\varphi = 0.05$, $K = 9$, $\beta = 0.2$, $n = 0.08$, $b = 0.7$, $c = 0.4$, $\delta = 0.35$, $a_1 = 0.2$, $a_2 = 1.8$, and (a) $ET = 1.8$; (b) $ET = 2.7$; (c) $ET = 4.2$. As ET increases, the stable focus E_R^{22} collides with the tangency point T_2 to form the boundary equilibrium E_B^2, which subsequently bifurcates into the pseudo-equilibrium E_{p_1}, the tangency point T_2, and the virtual equilibrium E_V^{22}.

When $c\beta - b\delta < 0$, another type of boundary-focus bifurcation may also occur. Under this condition, subsystem S_1 has no interior coexistence equilibrium point and only admits a locally asymptotically

stable boundary equilibrium point $(K, 0)$. The local asymptotic stability of $(K, 0)$ in subsystem S_1 implies that, in the absence of artificial control, the natural-enemy population eventually goes extinct, and the pest population tends to the environmental carrying capacity K. In contrast, the stability of the positive equilibrium E_R^{22} in subsystem S_2 reveals that pest-natural enemy coexistence can be sustained only via the combined action of pesticide application and continuous natural-enemy release.

From Figure 9(a), when $ET = 1.8$, the system has a stable focus E_R^{22}, a saddle point E_V^{21}, and a boundary equilibrium point E_V^{10}. This indicates that, under a relatively low economic threshold, control measures can take effect earlier, causing the pest and natural enemy populations to eventually achieve stable coexistence and thereby reducing the risk of sustained pest growth.

As shown in Figure 9(b), as ET increases to 2.7, the stable focus E_R^{22} coincides with the tangency point T_2, and the boundary equilibrium point E_B^2 emerges, indicating that the system is in a critical control state.

From Figure 9(c), when $ET = 4.2$, the boundary equilibrium point E_B^2 splits into a pseudo-equilibrium point E_{p_1}, a tangency point T_2, and a virtual equilibrium point E_V^{22}. Although subsystem S_1 has no interior equilibrium point, the adopted control strategy can still regulate the pest density around the prescribed economic threshold ET over an extended period and prevent it from approaching the carrying capacity K.

The above analysis shows that boundary bifurcations play an important role in the Filippov system. The pest population is initially stabilized at a real equilibrium point, namely the node E_R^1 or the focuses E_R^2 and E_R^{22}. As the economic threshold ET decreases or increases, the pest population undergoes a boundary bifurcation and eventually remains on Σ_s, which helps avert severe pest outbreaks.

5.3. Global sliding bifurcation

As the parameter ET varies, the system (2.4) may admit standard periodic solutions located in G_1 (or G_2), sliding periodic solutions containing part or all of the sliding segment, and crossing periodic solutions that only pass through the switching boundary.

Touching bifurcation: As shown in Figure 10(a), when $ET = 6.5$, the system admits a stable periodic solution entirely contained in G_1. Numerical simulations show that the system trajectories eventually converge to this stable standard periodic solution. In this case, the pest density remains below the control threshold throughout the periodic oscillations, indicating that the pest-natural enemy system can sustain stable fluctuations through natural predation alone, without the need for additional control measures.

When $ET = 5.78$, the standard periodic solution becomes tangent to the switching boundary at the tangency point T_1, and the system undergoes a touching bifurcation, as shown in Figure 10(b). In this critical case, the peak pest density just reaches the economic threshold, indicating that the system lies at the boundary between natural regulation and artificial intervention.

When $ET = 5.65$, the standard periodic solution is transformed into a sliding periodic solution containing a segment of the sliding region Σ_s, as shown in Figure 10(c). In this regime, pesticide spraying and natural enemy release act jointly to constrain the pest population near the economic threshold.

Buckling bifurcation: From Figure 10(c) and Figure 10(d), it can be seen that when ET decreases from 5.65 to 5.4, the sliding periodic solution that originally contains only part of the sliding segment Σ_s is transformed into a periodic solution containing the entire sliding segment Σ_s. When $ET = 4.9$,

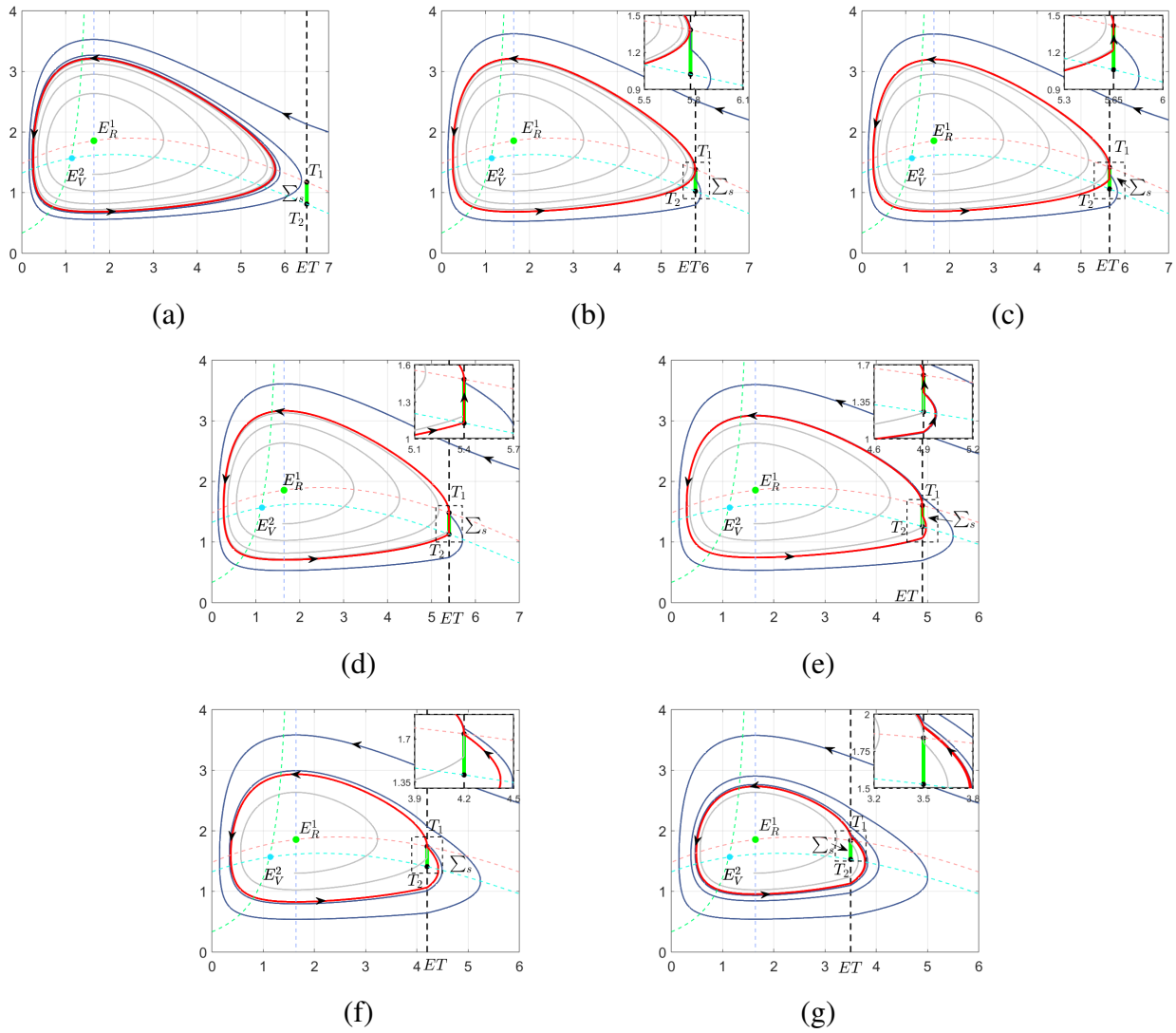

Figure 10. Global sliding bifurcation of system (2.4). As ET decreases, the system undergoes a transition from a standard periodic solution to a sliding periodic solution and finally to a crossing periodic solution. Parameters are: $r = 1$, $\varphi = 0.2$, $K = 10$, $\beta = 0.6$, $n = 0.13$, $b = 0.5$, $c = 0.6$, $\delta = 0.3$, $a_1 = 0.1$, $a_2 = 0.1$, and (a) $ET = 6.5$; (b) $ET = 5.78$; (c) $ET = 5.65$; (d) $ET = 5.4$; (e) $ET = 4.9$; (f) $ET = 4.2$; (g) $ET = 3.5$.

the sliding periodic solution begins to include the region G_2, as shown in Figure 10(e). At this point, the pest population not only slides near the threshold boundary, but also enters the dynamical region G_2 corresponding to the system after the implementation of control measures.

Crossing bifurcation: When $ET = 4.9$, the sliding periodic solution contains the sliding segment Σ_s and partial regions of G_1 and G_2, as shown in Figure 10(e). When $ET = 4.2$, the sliding periodic solution remains in contact with the upper tangency point of the sliding segment Σ_s, as shown in Figure 10(f). When $ET = 3.5$, the periodic solution no longer intersects the sliding segment and is transformed into a crossing periodic solution distributed in the regions G_1 and G_2, as shown in Figure 10(g). At this point, the pest density is no longer continuously maintained near the economic

threshold, but repeatedly switches between the uncontrolled and controlled states. Fixing $ET = 1.2$, the crossing bifurcation process of the system can also be observed by reducing the pesticide-induced per capita mortality rate a_1, as shown in Figure 11.

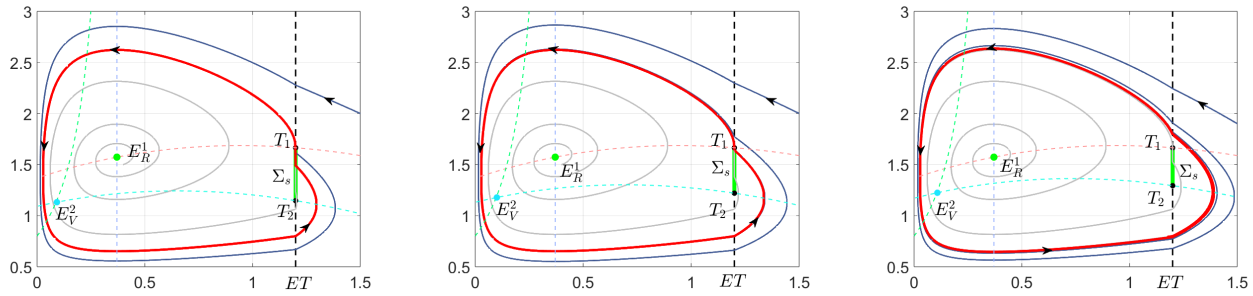

(a) (b) (c)

Figure 11. Another crossing bifurcation in system (2.4). Parameter values: $r = 0.7$, $\varphi = 0.1$, $K = 3.5$, $\beta = 0.5$, $n = 0.1$, $b = 1$, $c = 0.8$, $\delta = 0.1$, $a_2 = 0.08$, $ET = 1.2$, and (a) $a_1 = 0.14$; (b) $a_1 = 0.12$; (c) $a_1 = 0.1$.

These sliding bifurcation phenomena indicate that the selection of the threshold is crucial for intermittent pest control strategies. When the threshold is too high, the pest population fluctuates between natural growth and predation by natural enemies. When the threshold is appropriately reduced, control measures can suppress the pest population near the economic threshold. However, when the threshold is too low, the system frequently switches between the uncontrolled and controlled regions, thereby increasing control costs and ecological pressure. Therefore, the selection of the economic threshold should balance pest control effectiveness, economic investment, and ecological stability.

6. Impact of fear effect and global sensitivity analysis

6.1. *The impact of the fear effect on S_2*

This subsection examines how the fear-response coefficient φ affects the dynamics of system S_2. With all other parameters and initial values fixed, we present the time series of the pest population x and the natural enemy population y for $\varphi = 0.3, 0.7$, and 1.5, respectively. As shown in Figure 12(a), a small value of φ leads to stable periodic oscillations. When φ increases, the oscillation amplitude gradually decreases; see Figure 12(b). For $\varphi = 1.5$, both populations converge to a stable positive equilibrium, as illustrated in Figure 12(c). These results indicate that a sufficiently strong fear response can suppress population fluctuations in subsystem S_2 and help maintain ecological balance.

6.2. *Global sensitivity analysis*

Global sensitivity analysis was performed for subsystem S_2 using the partial rank correlation coefficient (PRCC) method combined with maximin Latin hypercube sampling (LHS). A total of 1000 parameter sets were generated with a fixed random seed of 1. The sampling ranges were $r \in [1.4, 2.6]$, $K \in [5.5, 10.5]$, $\varphi \in [0.1, 0.5]$, $\beta \in [0.7, 1.2]$, $b \in [0.2, 0.4]$, $n \in [0, 0.5]$, $c \in [0.5, 0.9]$,

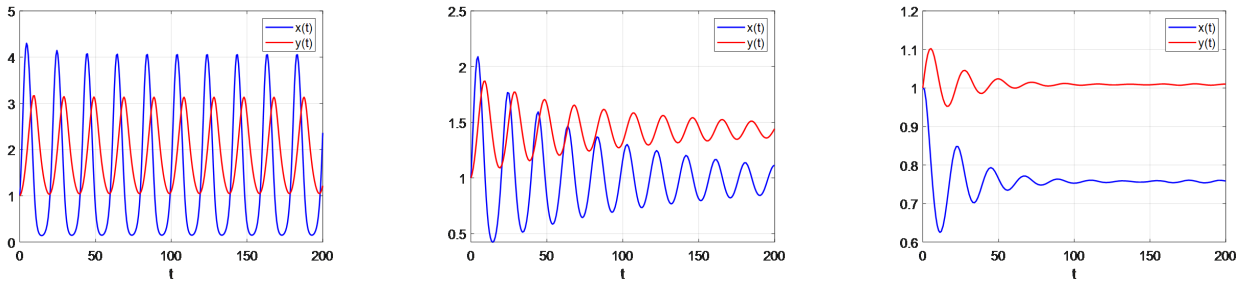

(a) (b) (c)

Figure 12. Time sequence diagram of system S_2, with parameter values $r = 1.5$, $K = 12$, $\beta = 0.65$, $n = 0.15$, $b = 0.6$, $c = 0.5$, $\delta = 0.25$, $a_1 = 0.1$, $a_2 = 0.1$, and (a) $\varphi = 0.3$; (b) $\varphi = 0.7$; (c) $\varphi = 1.5$. Increasing the fear-response coefficient φ reduces the oscillation amplitude and eventually promotes convergence to a stable positive equilibrium.

$\delta \in [0.3, 0.7]$, $a_1 \in [0.1, 0.4]$, and $a_2 \in [0.05, 0.30]$. For each parameter set, subsystem S_2 was numerically solved over $t \in [0, 200]$, with the initial condition $(x(0), y(0)) = (0.5, 0.5)$. The output variables were the time-averaged pest density $\bar{x}$ and natural-enemy density $\bar{y}$ over $t \in [150, 200]$. PRCC values and their two-sided p-values were calculated after rank transformation, and $p < 0.01$ was considered statistically significant.

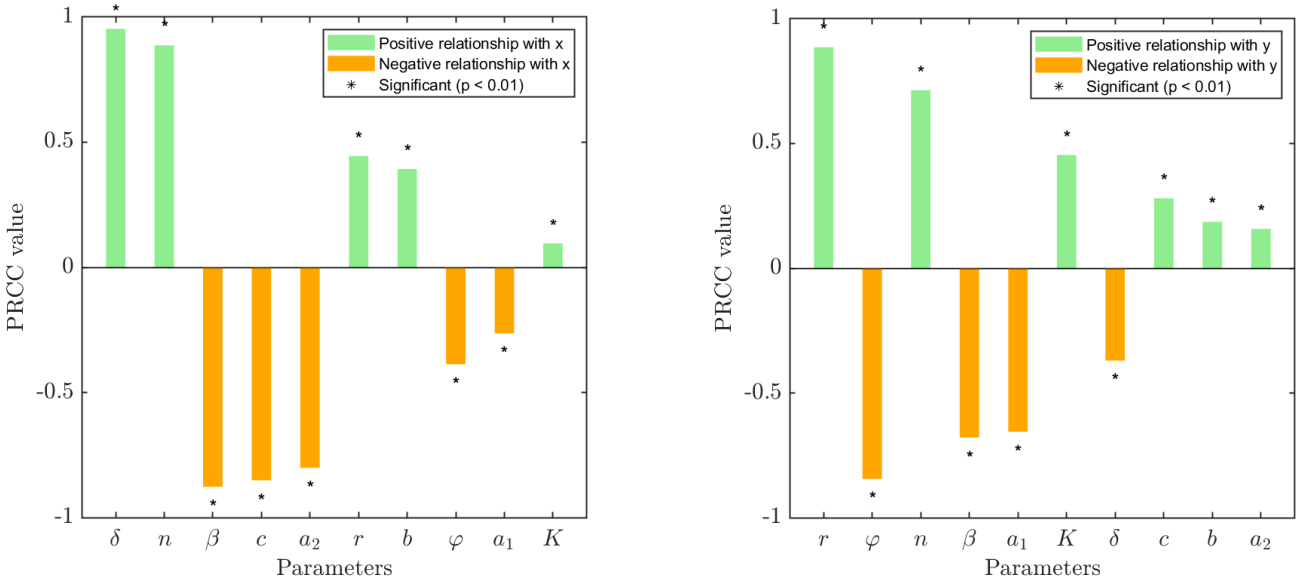

(a) (b)

Figure 13. PRCCs of the model parameters for (a) the time-averaged pest density $\bar{x}$ and (b) the time-averaged natural-enemy density $\bar{y}$, obtained from 1000 maximin Latin hypercube samples. Asterisks denote statistically significant correlations based on two-sided tests ($p < 0.01$).

From the PRCC-based parameter sensitivity analysis, the refuge coefficient n is positively correlated with the pest population size, indicating that a higher refuge proportion allows more pests

to escape predation by natural enemies, thereby promoting pest persistence and leading to an increase in pest density.

The pesticide-induced per capita mortality rate a_1 is negatively correlated with the pest population, indicating that increasing pesticide concentration can effectively suppress pests. However, excessive pesticide use may also inhibit the growth of natural enemies. Therefore, pesticide concentration should be carefully controlled to reduce pests while avoiding adverse effects on natural enemies.

The constant natural-enemy release rate a_2 is inversely related to the pest population but positively associated with the natural enemy population, implying that artificial augmentation of natural enemies is effective in reducing pest abundance and enhancing the persistence of natural enemy populations.

The fear-effect intensity φ has a significant inhibitory effect on the pest population, indicating that the presence of natural enemies not only suppresses pests through direct predation but also reduces pest growth through behavioral intimidation. However, φ is also negatively correlated with the natural enemy population, suggesting that an excessively strong fear effect may reduce the food resources available to natural enemies by suppressing pest activity and population growth.

7. Conclusions

The objective of pest control strategies is to maintain pest population density below the economic threshold while balancing ecological benefits and control costs. However, pests are not only directly affected by natural enemies and pesticides, but may also exhibit fear responses when perceiving predation risk and reduce their risk of being preyed upon through refuge behavior, thereby posing new challenges to the formulation and implementation of pest control strategies. Therefore, taking pest population density as the control index, this paper constructs a Filippov integrated pest management model that simultaneously incorporates the fear effect and prey refuge.

First, the positivity and boundedness of the system solutions are proved, and the dynamical properties of S_1 and S_2 are analyzed. On this basis, the sliding-mode dynamics of model (2.4) are further investigated, with a classified discussion of the existence intervals of sliding segments and the existence conditions for various types of equilibria. Subsequently, the sliding-mode bifurcation phenomena induced by changes in the economic threshold ET under different parameter conditions are explored. The results show that appropriately increasing the pesticide application concentration or the release rate of natural enemies helps maintain the existence of the pseudo-equilibrium point in the model. In contrast, an increase in the refuge coefficient causes the pseudo-equilibrium point to gradually move away from the sliding segment, thereby weakening the effectiveness of the integrated control strategy in regulating the pest population.

Numerical simulation results show that, as the economic threshold ET varies, the real equilibrium point and the tangency point of the system may collide, forming a boundary equilibrium point on the switching boundary and thereby inducing boundary-node and boundary-focus bifurcations. This paper also investigates the boundary bifurcation phenomena that occur when the subsystem has no interior equilibrium point. The results show that, compared with a higher economic threshold, appropriately lowering the economic threshold enables pest control measures to intervene earlier, thereby promoting the stable coexistence of pest and natural enemy populations and effectively reducing the risk of the pest population continuously increasing toward the environmental carrying capacity K. In addition, as ET gradually decreases, the system undergoes global sliding bifurcations and generates different

types of periodic solutions. These results indicate that the choice of the economic threshold is of great significance for intermittent pest control strategies: An excessively high threshold may lead to delayed intervention of control measures and thus weaken the control effect, whereas an excessively low threshold may cause frequent switching of the system and consequently increase control costs.

To further reveal the effects of key parameters on the population dynamics of pests and natural enemies, a parameter sensitivity analysis of system (3.2) is conducted. The results show that the refuge behavior of pests allows more pests to escape predation by natural enemies, thereby increasing pest population density. The sensitivity analysis further reveals a trade-off associated with the fear effect. Although fear effect can assist pest control by suppressing pest activity and population growth, an excessively strong fear response may reduce the food resources available to natural enemies and consequently decrease their population size. Therefore, the potential trade-off between pest suppression and natural enemy persistence should be taken into account when evaluating integrated pest management strategies.

In real ecological systems, the predation effect after the release of natural enemies and the efficacy of pesticides after application usually involve a certain time delay and do not take effect instantaneously. Therefore, based on the model proposed in this paper, time-delay factors may be further introduced in future work to investigate the influence of time-delay effects on the dynamical behavior of the Filippov integrated pest management model, thereby making the model more consistent with practical pest control processes.

Use of AI tools declaration

The authors declare they have not used Artificial Intelligence (AI) tools in the creation of this article.

Acknowledgments

This work was supported by The National Natural Science Foundation of China (Grant No. 12261033). The authors would like to thank the editor and anonymous referees for their valuable comments and suggestions which have led to an improvement of the paper.

Conflict of interest

The authors declare there are no conflicts of interest.

References

1. N. Y. Su, R. H. Scheffrahn, A review of subterranean termite control practices and prospects for integrated pest management programmes, *Integr. Pest Manag. Rev.*, **3** (1998), 1–13. https://doi.org/10.1023/A:1009684821954
2. J. Pretty, Z. P. Bharucha, Integrated pest management for sustainable intensification of agriculture in Asia and Africa, *Insects*, **6** (2015), 152–182. https://doi.org/10.3390/insects6010152
3. M. Kogan, Integrated pest management: Historical perspectives and contemporary developments, *Annu. Rev. Entomol.*, **43** (1998), 243–270. https://doi.org/10.1146/annurev.ento.43.1.243

4. P. B. Angon, S. Mondal, I. Jahan, M. Datto, U. B. Antu, F. J. Ayshi, et al., Integrated pest management (ipm) in agriculture and its role in maintaining ecological balance and biodiversity, *Adv. Agric.*, **2023** (2023), 5546373. https://doi.org/10.1155/2023/5546373

5. C. Cortés-García, Population dynamics of a Filippov Gause predator-prey model with or without competition among predators with respect to prey density, *Nonlinear Dyn.*, **113** (2025), 30161–30185. https://doi.org/10.1007/s11071-025-11600-7

6. C. Cortés-García, Dynamics in a Filippov-Gause predator-prey model with hunting cooperation or competition among predators for high or low prey densities, *Int. J. Bifurcation Chaos*, **35** (2025), 2550014. https://doi.org/10.1142/S0218127425500142

7. C. Cortés-García, Population dynamics in a Leslie-Gower predator-prey model with predator harvesting at high densities, *Math. Methods Appl. Sci.*, **48** (2025), 804–838. https://doi.org/10.1002/mma.10359

8. W. Qin, S. Tang, C. Xiang, Y. Yang, Effects of limited medical resource on a Filippov infectious disease model induced by selection pressure, *Appl. Math. Comput.*, **283** (2016), 339–354. https://doi.org/10.1016/j.amc.2016.02.042

9. Y. Zhang, Y. Xiao, Global dynamics for a Filippov epidemic system with imperfect vaccination, *Nonlinear Anal. Hybrid Syst.*, **38** (2020), 100932. https://doi.org/10.1016/j.nahs.2020.100932

10. A. Wang, Y. Xiao, A Filippov system describing media effects on the spread of infectious diseases, *Nonlinear Anal. Hybrid Syst.*, **11** (2014), 84–97. https://doi.org/10.1016/j.nahs.2013.06.005

11. X. Zhang, Z. Xiang, Impact of combined effects of vectors, protective measures, and vaccination under threshold policy control on the SISV model, *Chaos*, **35** (2025), 053117. https://doi.org/10.1063/5.0256966

12. X. Jiao, X. Liu, Rich dynamics of a delayed Filippov avian-only influenza model with two-thresholds policy, *Chaos Solitons Fractals*, **182** (2024), 114710. https://doi.org/10.1016/j.chaos.2024.114710

13. W. Li, Bifurcation analysis of a filippov predator-prey model with two thresholds, *Nonlinear Dyn.*, **112** (2024), 9639–9656. https://doi.org/10.1007/s11071-024-09527-6

14. M. Hu, C. Xiang, B. Chu, Dynamic behaviors and bifurcation analysis of a three-dimensional filippov ecosystem with fear effect, *Math. Methods Appl. Sci.*, **48** (2025), 6607–6623. https://doi.org/10.1002/mma.10699

15. X. Zhang, X. Zhang, Complex dynamics analysis of a non-smooth predator-prey model with stage structure and threshold-dependent refuge mechanism, *Nonlinear Dyn.*, **114** (2026), 533. https://doi.org/10.1007/s11071-026-12405-y

16. Z. Xiang, X. Zhang, Application of a Filippov model incorporating the Allee effect and proportional release of sterile mosquitoes for dengue mosquito population control, *Commun. Nonlinear Sci. Numer. Simul.*, **154** (2026), 109590. https://doi.org/10.1016/j.cnsns.2025.109590

17. D. M. Fawzy, A. Elsaid, W. Zahra, A. A. Arafa, Qualitative analysis of a Filippov wild-sterile mosquito population model with immigration, *Chaos*, **33** (2023), 113101. https://doi.org/10.1063/5.0167157

18. H. Zhou, Q. Zhang, S. Tang, Qualitative analysis of the sliding vector field in a Filippov food chain model with integrated pest management strategy, *Appl. Math. Comput.*, **490** (2025), 129188. https://doi.org/10.1016/j.amc.2024.129188

19. Y. Tian, X. Tian, X. Yan, J. Zheng, K. Sun, Complex dynamics of non-smooth pest-natural enemy Gomportz models with a variable searching rate based on threshold control, *Electron. Res. Arch.*, **33** (2025), 26–49. https://doi.org/10.3934/era.2025002

20. Y. Tian, H. Guo, W. Shen, X. Yan, J. Zheng, K. Sun, Dynamic analysis and validation of a prey-predator model based on fish harvesting and discontinuous prey refuge effect in uncertain environments, *Electron. Res. Arch.*, **33** (2025), 973–994. https://doi.org/10.3934/era.2025044

21. H. Zhou, X. Wang, S. Tang, Global dynamics of non-smooth filippov pest-natural enemy system with constant releasing rate, *Math. Biosci. Eng.*, **16** (2019), 7327–7361. https://doi.org/10.3934/mbe.2019366

22. W. Qin, X. Tan, M. Tosato, X. Liu Threshold control strategy for a non-smooth Filippov ecosystem with group defense, *Appl. Math. Comput.*, **362** (2019), 124532. https://doi.org/10.1016/j.amc.2019.06.046

23. B. Kang, X. Hou, B. Liu, Threshold control strategy for a Filippov model with group defense of pests and a constant-rate release of natural enemies, *Math. Biosci. Eng.*, **20** (2023), 12076–12092. https://doi.org/10.3934/mbe.2023537

24. A. A. Arafa, S. A. Hamdallah, S. Tang, Y. Xu, G. M. Mahmoud, Dynamics analysis of a filippov pest control model with time delay, *Commun. Nonlinear Sci. Numer. Simul.*, **101** (2021), 105865. https://doi.org/10.1016/j.cnsns.2021.105865

25. L. Y. Zanette, A. F. White, M. C. Allen, M. Clinchy, Perceived predation risk reduces the number of offspring songbirds produce per year, *Science*, **334** (2011), 1398–1401. https://doi.org/10.1126/science.1210908

26. X. Wang, L. Zanette, X. Zou, Modelling the fear effect in predator-prey interactions, *J. Math. Biol.*, **73** (2016), 1179–1204. https://doi.org/10.1007/s00285-016-0989-1

27. M. A. Abbasi, M. Samreen, Analyzing multi-parameter bifurcation on a prey-predator model with the allee effect and fear effect, *Chaos Solitons Fractals*, **180** (2024), 114498. https://doi.org/10.1016/j.chaos.2024.114498

28. Y. Li, M. He, Z. Li, Dynamics of a ratio-dependent Leslie-Gower predator-prey model with allee effect and fear effect, *Math. Comput. Simul.*, **201** (2022), 417–439. https://doi.org/10.1016/j.matcom.2022.05.017

29. H. Qi, B. Liu, Stationary distribution of a stochastic reaction-diffusion predator-prey model with additional food and fear effect, *Appl. Math. Lett.*, **150** (2024), 108978. https://doi.org/10.1016/j.aml.2023.108978

30. H. Wang, Y. Zhang, L. Ma, Bifurcation and stability of a diffusive predator-prey model with the fear effect and time delay, *Chaos*, **33** (2023), 073137. https://doi.org/10.1063/5.0157410

31. O. Akman, T. Comar, M. Henderson, An analysis of an impulsive stage structured integrated pest management model with refuge effect, *Chaos Solitons Fractals*, **111** (2018), 44–54. https://doi.org/10.1016/j.chaos.2018.03.039

32. Y. Cai, Q. Chen, Z. Teng, G. Zhang, R. Rifhat, Bifurcations in a discrete-time Beddington-DeAngelis prey-predator model with fear effect, prey refuge and harvesting, *Nonlinear Dyn.*, **113** (2025), 931–969. https://doi.org/10.1007/s11071-024-10232-7
33. T. K. Kar, Stability analysis of a prey-predator model incorporating a prey refuge, *Commun. Nonlinear Sci. Numer. Simul.*, **10** (2005), 681–691. https://doi.org/10.1016/j.cnsns.2003.08.006
34. W. Ko, K. Ryu, Qualitative analysis of a predator-prey model with Holling type ii functional response incorporating a prey refuge, *J. Differ. Equations*, **231** (2006), 534–550. https://doi.org/10.1016/j.jde.2006.08.001
35. M. Venzon, A. Janssen, A. Pallini, M. W. Sabelis, Diet of a polyphagous arthropod predator affects refuge seeking of its thrips prey, *Anim. Behav.*, **60** (2000), 369–375. https://doi.org/10.1006/anbe.2000.1483
36. S. Magalhaes, P. C. Van Rijn, M. Montserrat, A. Pallini, M. W. Sabelis, Population dynamics of thrips prey and their mite predators in a refuge, *Oecologia*, **150** (2007), 557–568. https://doi.org/10.1007/s00442-006-0548-3
37. K. Mokni, M. Ch-Chaoui, Strong Allee effect and evolutionary dynamics in a single-species Ricker population model, *J. Biol. Syst.*, **31** (2023), 1341–1370. https://doi.org/10.1142/S0218339023500456
38. K. Mokni, M. Ch-Chaoui, Exploring persistence, stability, and bifurcations: A Darwinian Ricker-Cushing model, *Int. J. Dyn. Control*, **13** (2025), 34. https://doi.org/10.1007/s40435-024-01539-9
39. M. Ahmidi, K. Mokni, M. Ch-Chaoui, Influence of prey harvesting on the dynamics of a prey-predator system: Multi-parameter bifurcation analysis, *Nonlinear Dyn.*, **113** (2025), 31841–31870. https://doi.org/10.1007/s11071-025-11701-3
40. H. Benali, K. Mokni, H. Mouhsine, M. Ch-Chaoui, Unveiling complexity: A discrete-time prey-predator model with immigration effects, *Iran J. Sci.*, **49** (2025), 449–462. https://doi.org/10.1007/s40995-024-01742-5
41. H. Zhang, Y. Cai, S. Fu, W. Wang, Impact of the fear effect in a prey-predator model incorporating a prey refuge, *Appl. Math. Comput.*, **356** (2019), 328–337. https://doi.org/10.1016/j.amc.2019.03.034
42. S. A. Hamdallah, A. A. Arafa, Stability analysis of Filippov prey-predator model with fear effect and prey refuge, *J. Appl. Math. Comput.*, **70** (2024), 73–102. https://doi.org/10.1007/s12190-023-01934-z

AIMS Press